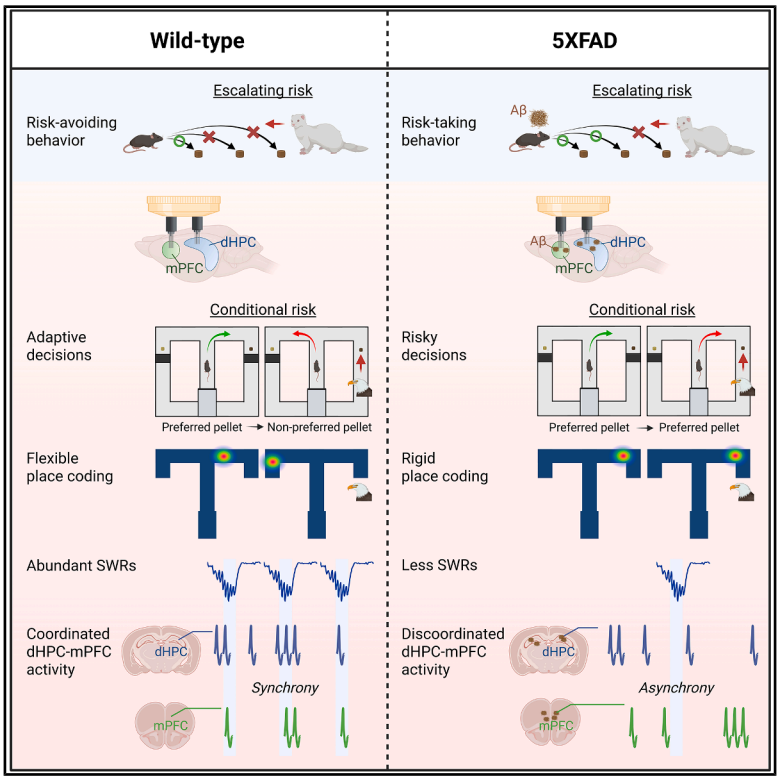
Cell Reports

Disruption of hippocampal-prefrontal neural dynamics and risky decision-making in a mouse model of Alzheimer's disease

Graphical abstract



Highlights

- 5XFAD mice exhibit impaired risky decision-making in ecologically valid paradigms
- Amyloid pathology disrupts place cell flexibility and reduces sharp-wave ripple activity
- SWR-associated corticolimbic coordination is impaired in 5XFAD mice
- Hippocampal-prefrontal synchrony is diminished in 5XFAD mice

Authors

Eun Joo Kim, Sanggeon Park, Bryan P. Schuessler, Harry Boo, Jeiwon Cho, Jeansok J. Kim

Correspondence

ejkim731@uw.edu (E.J.K.), jelectro21@ewha.ac.kr (J.C.), jeansokk@uw.edu (J.J.K.)

In brief

Kim et al. show that 5XFAD mice exhibit persistent risk-taking and reduced behavioral flexibility in naturalistic "approach food-avoid predator" foraging paradigms. Simultaneous neural recordings reveal rigid place cell coding, impaired SWR-associated corticolimbic coordination, and disrupted hippocampal-prefrontal synchrony, linking Alzheimer's disease pathology to deficits in adaptive decision-making.

Kim et al., 2025, Cell Reports *44*, 116081
August 26, 2025 © 2025 The Author(s). Published by Elsevier Inc.
https://doi.org/10.1016/j.celrep.2025.116081

CellPress

Cell Reports

CellPress
OPEN ACCESS

Report

Disruption of hippocampal-prefrontal neural dynamics and risky decision-making in a mouse model of Alzheimer's disease

Eun Joo Kim,[1,6,*] Sanggeon Park,[3,4,6] Bryan P. Schuessler,[1,5] Harry Boo,[1] Jeiwon Cho,[3,*] and Jeansok J. Kim[1,2,7,*]
[1]Department of Psychology, Seattle, WA 98195-1525, USA
[2]Neuroscience Program, University of Washington, Seattle, WA 98195-1525, USA
[3]Department of Brain and Cognitive Sciences, Scranton College, Ewha Womans University, Seoul 03760, Republic of Korea
[4]Brain Link Creative Research Section, Electronics and Telecommunications Research Institute (ETRI), Daejeon 34129, Republic of Korea
[5]VA Northwest Geriatric Research Education and Clinical Center, VA Puget Sound Health Care System, Seattle, WA 98108, USA
[6]These authors contributed equally
[7]Lead contact
*Correspondence: ejkim731@uw.edu (E.J.K.), jelectro21@ewha.ac.kr (J.C.), jeansokk@uw.edu (J.J.K.)
https://doi.org/10.1016/j.celrep.2025.116081

SUMMARY

This study investigates how amyloid pathology influences hippocampal-prefrontal neural dynamics and decision-making in Alzheimer's disease (AD) using 5XFAD mice, a well-established model system characterized by pronounced early amyloid pathology. Utilizing ecologically relevant "approach food-avoid predator" foraging tasks, we show that 5XFAD mice exhibit persistent risk-taking behaviors and reduced adaptability to changing threat conditions, indicative of impaired decision-making. Multi-regional neural recordings reveal rigid hippocampal CA1 place cell fields, decreased sharp-wave ripple (SWR) frequencies, and disrupted medial prefrontal-hippocampal connectivity, all of which correspond with deficits in behavioral flexibility during spatial risk scenarios. These findings highlight the critical role of SWR dynamics and corticolimbic circuit integrity in adaptive decision-making, with implications for understanding cognitive decline in AD in naturalistic contexts. By identifying specific neural disruptions underlying risky decision-making deficits, this work provides insights into the neural basis of cognitive dysfunction in AD and suggests potential targets for therapeutic intervention.

INTRODUCTION

Alzheimer's disease (AD) research has traditionally focused on memory impairment, yet growing evidence shows that AD also disrupts decision-making under risk and ambiguity,[1–10] functions essential for daily life. Notably, decision-making deficits may precede memory loss,[11–20] with early signs like reduced scam awareness and impaired financial judgment linked to amyloid accumulation and heightened AD risk.[11,19,21] Neuroeconomic studies in patients with early- to moderate-stage AD show impairments in risky decision-making,[20,22] suggesting that this domain may serve as an early behavioral marker. Unlike basic memory processes, decision-making integrates spatial context, emotional regulation, and experiences.[23–25] However, preclinical models remain limited[26] due to a lack of naturalistic behavioral paradigms.

Although AD pathology is generally defined by β-amyloid (Aβ) plaques and tau tangles, how these changes affect real-time neural circuit functions during behavior remains poorly understood. This gap persists despite the limited success of Aβ-targeted therapies[27–29] and evidence of cognitive resilience despite amyloid pathology.[30–32] These findings highlight the need to examine how AD disrupts neural connectivity during behavior.[33–35]

The medial prefrontal cortex (mPFC) and the dorsal hippocampus (dHPC) form a key circuit for decision-making. Damage or inactivation of either region impairs risk-based behavior in rodents, monkeys, and humans.[36–41] fMRI studies in humans and single-unit recordings in animals performing probabilistic/delay-discounting tasks link decision-making to mPFC and dHPC activity.[38,42] Patients with AD also show deficits in financial decision-making[22] and set-shifting tasks,[3] attributed to Aβ plaques and tau tangles in the dHPC and mPFC—regions particularly vulnerable to AD.

Despite these insights, risky decision-making within ecologically relevant paradigms and mPFC-dHPC dynamics remain unexplored in AD models. Our prior work in rats documented neural activity during goal-directed foraging in risky environments.[43,44] We found that dHPC place cells encoded spatial-danger gradients, with unstable firing near a predatory robot but stable firing near the safe nest, highlighting the dHPC's role in spatial-danger coding. Concurrently, mPFC neurons tracked food procurement and exhibited heightened activity during cautious approaches to a stationary predator, underscoring the mPFC's role in threat

This is an open access article under the CC BY-NC-ND license (http://creativecommons.org/licenses/by-nc-nd/4.0/).

assessment and decision-making. These findings highlight the value of naturalistic foraging paradigms to investigate risky choices[3,5,45] and mPFC-dHPC activity in AD models.

Here, we apply this approach to the 5XFAD transgenic mouse model, which develops Aβ pathology from ~4 months due to overexpression of amyloid precursor protein (APP) and presenilin 1 (PS1) mutations.[46–49] We focus on dHPC sharp-wave ripples (SWRs)—brief, high-frequency (150–250 Hz) oscillations linked to memory, emotion, and deliberation[50,51]—and their coordination with mPFC activity.[52–54] SWRs are reduced in APP/PS1,[55] apolipoprotein E4 knockin (KI),[56,57] and 5XFAD[58] models, with recent evidence linking these deficits to hippocampal inhibitory synaptic dysfunction.[59]

By leveraging naturalistic environments that influence and reshape neural activity and behavior,[60–63] we adapted the rat "approach food-avoid predator" conflict paradigm[64,65] to the 5XFAD model. This platform enables a comprehensive analysis of how AD affects cognition and mPFC-dHPC coordination during risky decision-making. Our study aims to provide new insights into the neural dynamics and behavioral alterations associated with risky decision-making in AD.

RESULTS

5XFAD mice exhibit risk-prone foraging with escalating predatory risk

5XFAD and wild-type (WT) mice were tested in a foraging task in which predatory risk increased with distance from a safe nest (Figure 1). The task consisted of three phases: nest habituation, baseline foraging, and predator testing. During baseline foraging, both 5XFAD and WT mice left the nest and retrieved food pellets in a large open arena (104 × 45 × 61 cm) with similar efficiency (Figure S1A). Notably, during the very first baseline trial—when mice encountered the open arena for the first time—trial-by-trial latencies showed similar hesitation following gate opening, as reflected in comparable nest-exit latencies. This suggests no genotype differences in baseline anxiety levels in response to a novel environment.

The day after the final baseline session, animals were exposed to a predator (a surging weasel) in the testing arena (Figures 1A and 1B). Behavioral patterns were consistent across sexes and age groups, allowing data to be pooled (Figures S1B and S1C). On the first day of predator testing, both groups initially fled to the nest in response to the surging weasel, with significantly longer pellet retrieval latencies at the longest distance (L; 38.1 cm) compared to baseline (Figures 1C and 1D). At the medium distance (M; 25.5 cm), WT mice displayed risk-averse behavior, whereas 5XFAD mice continued foraging, indicating risk-prone behavior. At the shortest distance (S; 12.7 cm), both groups successfully retrieved the pellet; WT latencies matched baseline, while 5XFAD mice showed shorter latencies. Across all distances, 5XFAD mice had shorter mean retrieval latencies than WT mice (Figure 1E).

Importantly, these latency differences were not accompanied by group differences in running speed (velocity), latency to enter the foraging area, or the number of pellet attempts (Figures 1F and S1D–S1F), suggesting preserved predator responsiveness and pellet motivation.

Histological analysis confirmed significantly elevated Aβ plaque deposits in the dCA1 and mPFC of 5XFAD mice relative to WT controls (Figures 1G–1I).

Together, these findings suggest that Aβ pathology in 5XFAD mice impairs the ability to assess threat levels and discern safety boundaries under escalating predatory risk, leading to risk-prone foraging behavior.

5XFAD mice exhibit inflexible foraging and rigid place cell coding in a conditional predatory task

To examine how Aβ pathology affects risky decision-making and hippocampal spatial coding, 5XFAD and WT mice were implanted with tetrode arrays in the dHPC (targeting the CA1 subregion) and mPFC ipsilaterally (Figure S2A). Mice were tested in a conditional foraging task within a T-shaped maze, where narrow pathways enhanced visit map reliability, and predator visibility was restricted to the pellet zone, enabling analysis of place cell responses to internal fear (threat anticipation) states. Mice progressed through nest habituation, baseline foraging, and predator testing, with distinct pellet types (grain based and chocolate flavored) placed in separate goal arms (Figure 2A). Neural recordings were collected during both pre-predator and predator sessions (Figure 2B).

During the predator session, the preferred pellet arm was rendered "risky" by pairing it with a looming predator. WT mice adapted by switching to the non-preferred, safe arm to avoid the threat (Figure 2C). In contrast, 5XFAD mice continued to visit the predator-associated arm, as reflected by significantly higher preference index (PI) values compared to WT mice (Figure 2D). Despite divergent foraging strategies, both groups reduced their movement speed during the predator session relative to pre-predator levels, indicating a generalized caution response. However, movement speeds did not differ significantly between genotypes in either session (Figure 2E). Histological analysis confirmed elevated Aβ plaque deposits in both dHPC and mPFC of 5XFAD mice (Figures S2B and S2C). These findings suggest that Aβ pathology disrupts behavioral flexibility under threat without affecting baseline locomotion or motivation to forage.

Building on previous research showing place cell remapping in proximity to predatory threats,[44,66] we examined how Aβ pathology affects spatial coding in 5XFAD mice (Figure 2F). Recordings were obtained from 6 WT (94 units) and 11 5XFAD (112 units) mice. Place cells were categorized by peak firing locations during the pre-predator session: nest cells (WT, n = 18; 5XFAD, n = 35), center-arm cells (WT, n = 24; 5XFAD, n = 24), risky-arm cells (WT, n = 14; 5XFAD, n = 19), and safe-arm cells (WT, n = 13; 5XFAD, n = 10) (Figure 2G).

WT mice exhibited significant remapping in risky- and center-arm cells, as indicated by lower spatial correlations (Z') compared to nest cells (Figure 2H), and increased peak distances in risky-arm cells (Figure 2I), consistent with flexible spatial coding in response to threat. In contrast, 5XFAD mice showed minimal remapping in these regions, reflected by higher spatial correlations and reduced peak shifts (Figures 2H, 2I, S2D, and S2E), indicating reduced neural flexibility and impaired spatial-fear encoding. Although the place field size in risky-arm cells was larger in 5XFAD mice during the pre-predator session

CellPress
OPEN ACCESS

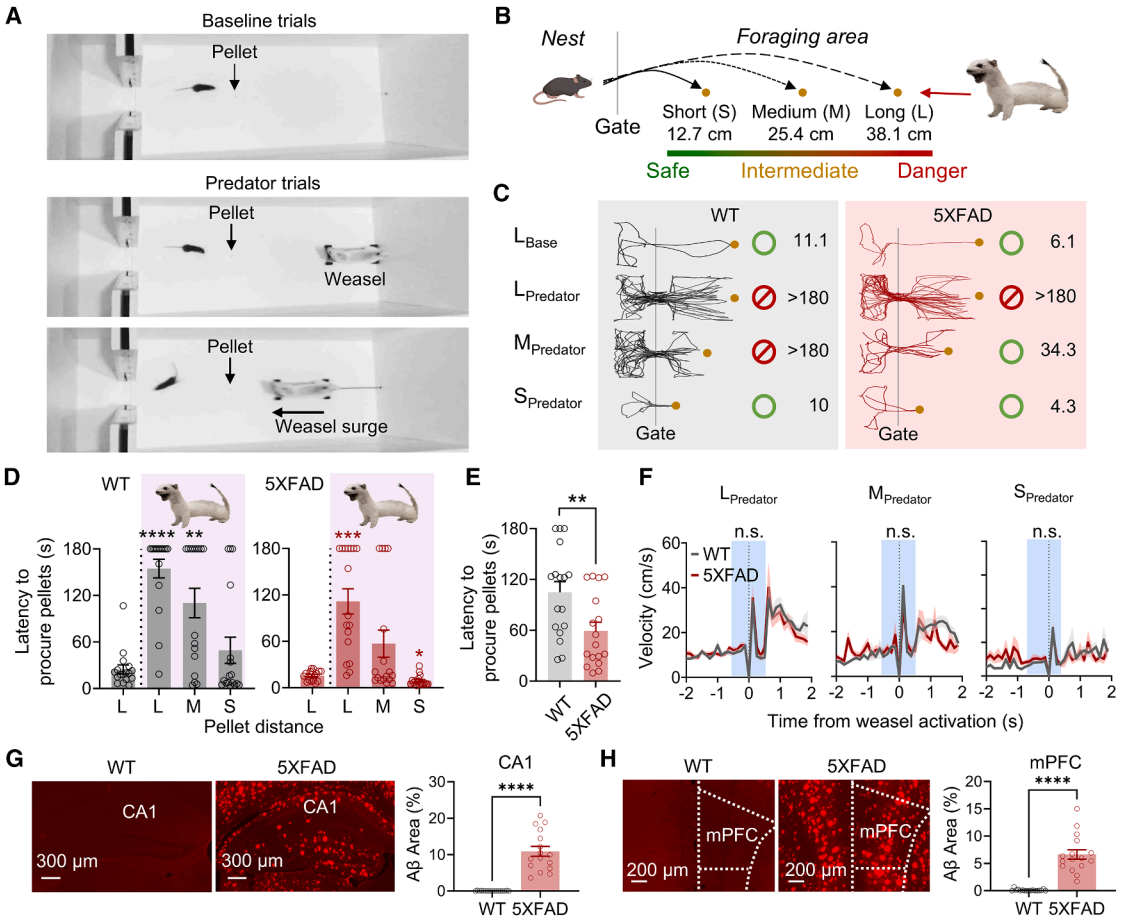


Figure 1. 5XFAD mice exhibit risk-prone foraging in an escalating predatory task

(A) Image of a foraging mouse encountering a predatory weasel.

(B) Schematic of the behavioral procedure.

(C) Representative foraging trajectories for WT and 5XFAD mice during predator testing.

(D) Latency to procure pellets in WT (n = 17, left) and 5XFAD (n = 17, right) mice.

(E) Mean latency to procure pellets across three weasel trials in WT and 5XFAD mice.

(F) Approach (prior to weasel activation) and escape (after weasel activation) velocities in WT and 5XFAD mice at long (L), medium (M), and short (S) distances (shaded area: −500 to +500 ms relative to weasel activation).

(G and H) Representative images showing Aβ plaque accumulation in the dCA1 (G, left and middle; scale bar, 300 μm) and mPFC (H, left and middle; scale bar, 200 μm) of a WT and a 5XFAD mouse and mean area percentage of Aβ accumulation in dCA1 (G, right) and mPFC (H, right) in WT and 5XFAD mice.

Data are presented as mean ± SEM. $^{**}p < 0.01$, $^{***}p < 0.001$, $^{****}p < 0.0001$. See also Figure S1.

(Figure S3A), it did not correlate with spatial correlation or peak distance (Figures S3B and S3C), suggesting that field size alone does not account for remapping deficits.

In the safe arm, place field stability resembled that of nest cells, with similar spatial correlation and peak distance values (Figures S3D and S3E). However, due to limited occupancy, especially in the safe arm during the pre-predator session (in most mice from both groups) and the predator session (in most 5XFAD mice), further analysis was not conducted for this zone.

In summary, 5XFAD mice persistently preferred risky zones and failed to adapt their foraging behavior in response to threat. Correspondingly, their place cells showed rigid spatial coding and failed to remap under dynamic threat conditions. These findings suggest that Aβ pathology impairs hippocampal encoding of threat-relevant spatial information and disrupts adaptive decision-making in ecologically relevant contexts.

5XFAD mice exhibit altered SWRs and disrupted SWR-associated dHPC activity during foraging under predatory risks

We analyzed SWRs and dHPC neuronal activity during foraging under predatory risks. Both 5XFAD and WT mice exhibited SWRs (Figure 3A), but 5XFAD mice showed a significantly reduced dCA1 SWR frequency across all sessions (Figure 3B, left). SWR durations were similar between groups, with both showing longer SWRs during predator sessions compared to pre-predator sessions (Figure 3B, right). The majority of SWRs

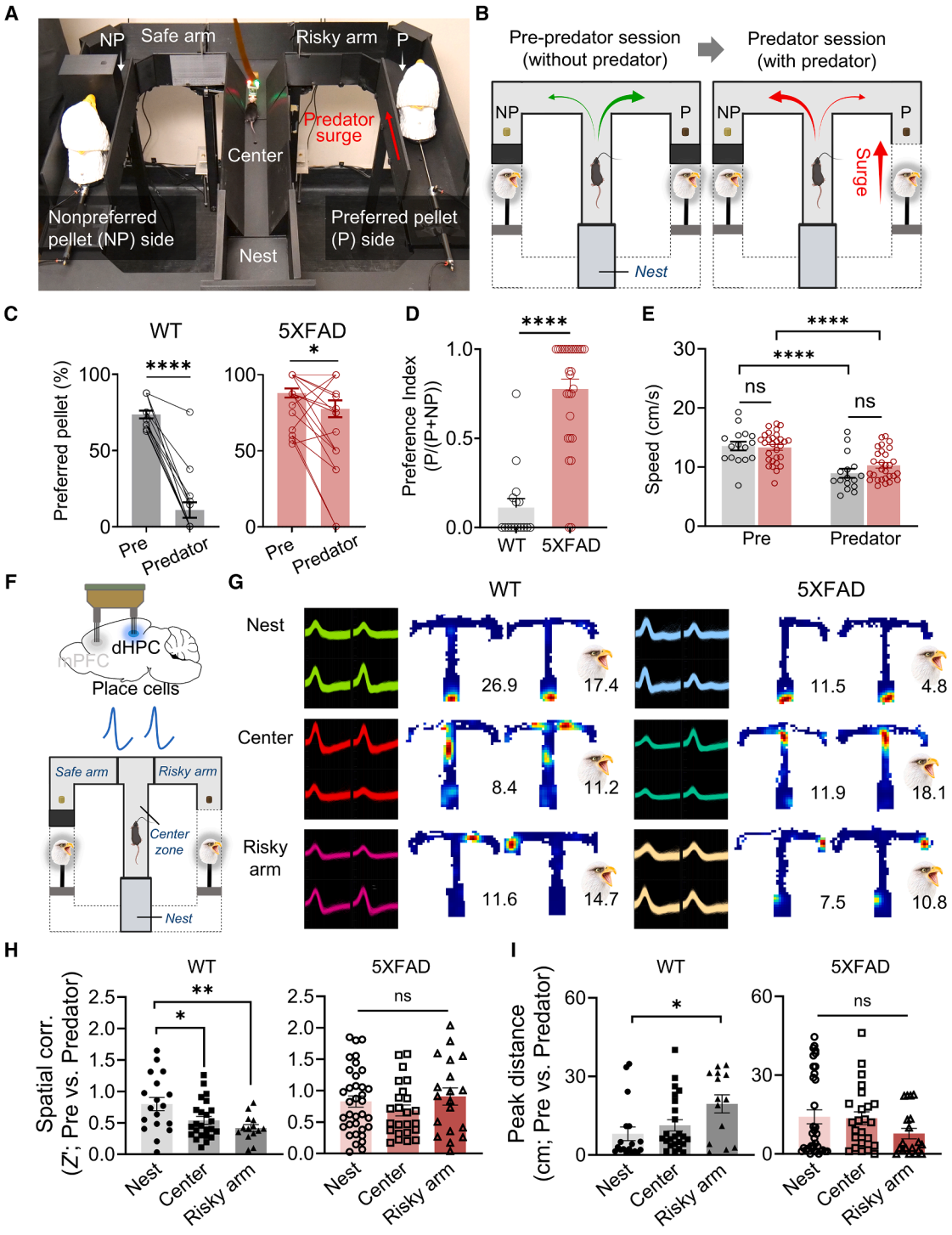


Figure 2. 5XFAD mice exhibit inflexible foraging and rigid place cell coding in a conditional predatory task

(A) Image of a mouse tethered for neural recording in the T maze apparatus.

(B) Schematic of the behavioral procedure consisting of successive pre-predator and predator sessions.

(C) Comparison of successful procurement of preferred (P) and non-preferred (NP) pellets between pre-predator and predator sessions in WTs (6 mice, 16 recording days) and 5XFADs (11 mice, 29 recording days).

(D) PI (ratio of preferred pellet choices to total choices) during the predator session in WT and 5XFAD mice.

(E) Overall movement speed during pre-predator and predator sessions in WT and 5XFAD mice.

(F) Tetrode recordings of dHPC place cells (top) and designated zones in the T maze (bottom): nest, center zone, risky arm, and safe arm.

(legend continued on next page)

CellPress
OPEN ACCESS

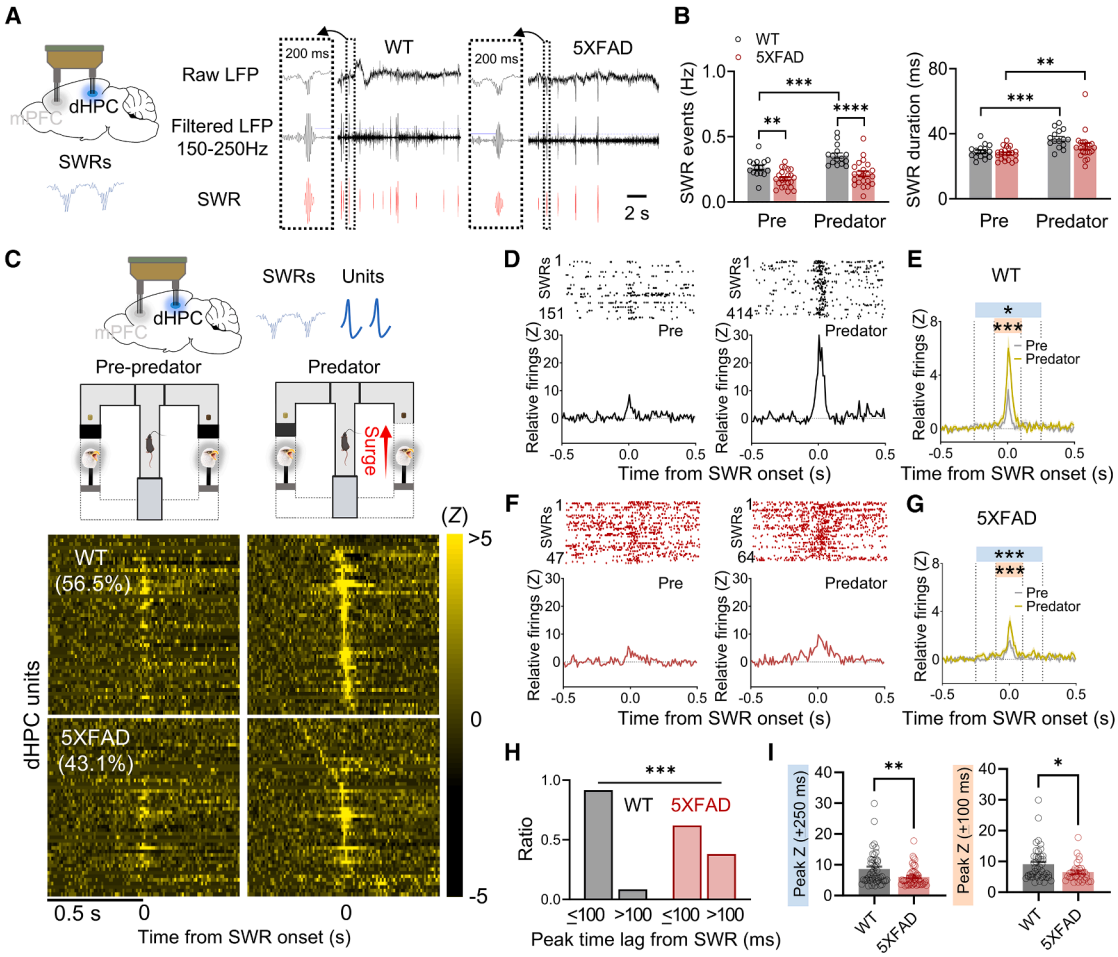


Figure 3. 5XFAD mice exhibit alterations in SWRs and associated dHPC activity during foraging under predatory risk

(A) Representative recordings of dHPC SWR activity from a WT and a 5XFAD mouse.

(B) Mean SWR frequency (left) and duration (right) in WT and 5XFAD mice across sessions.

(C) Top: dHPC SWR and unit activity analyzed across sessions. Bottom: color-coded activity (*Z* scores) of significantly firing dHPC units during peri-SWR epochs in predator trials, aligned to SWR onset for each session.

(D and E) Representative (D) and group (E) peri-SWR activity (mean *Z* scores) of WT dHPC neurons showing significant firing ($Z > 3$) within the ±250 ms period around SWR onset during the predator session. Mean *Z* scores during the ±250 ms (blue) and ±100 ms (orange) periods were compared across sessions.

(F and G) Representative (F) and group (G) peri-SWR activity of 5XFAD dHPC neurons as in (D and E).

(H) Proportions of dHPC neurons exhibiting significant activity within the ±250 ms vs. ±100 ms periods, compared between WT and 5XFAD groups.

(I) SWR-related dHPC cell activity (peak *Z* scores within the ±250 ms and ±100 ms periods) during the predator session in WT and 5XFAD mice.

Data are presented as mean ± SEM. $^{*}p < 0.05$, $^{**}p < 0.01$, $^{***}p < 0.001$, $^{****}p < 0.0001$. See also Figures S4–S6.

were detected in the nest area, with relatively few events recorded elsewhere (Figure S4A), indicating that the reported SWR differences primarily reflect dynamics within the nest. Given prior evidence that dHPC SWR-associated reactivation supports general, rather than trial-specific, information processing,[67] our findings suggest that SWR-related integration may occur continuously throughout the session.

To assess SWR modulation of dHPC firing, we analyzed peri-SWR activity (±250 ms around SWR onset) during both pre-predator and predator sessions (Figure 3C). The proportion of dHPC units exhibiting significant peri-SWR firing ($Z > 3$) during the predator session was similar for WT (56.5%) and 5XFAD (43.1%) mice. Both groups displayed higher firing rates within the ±250 ms and ±100 ms windows during predator sessions

(G) Representative waveforms and place fields from nest, center-, and risky-arm cells during pre-predator and predator sessions in WT (left) and 5XFAD (right) mice. The color scale (red, maximal firing; blue, no spikes) represents the firing rate for each unit; numerical values indicate peak firing rates per session.

(H and I) Spatial correlations (H) and peak distances (I) between pre-predator and predator sessions within the nest, center-, and risky-arm zones.

Data are presented as mean ± SEM. $^{*}p < 0.05$, $^{**}p < 0.01$, $^{****}p < 0.0001$. See also Figures S2 and S3.

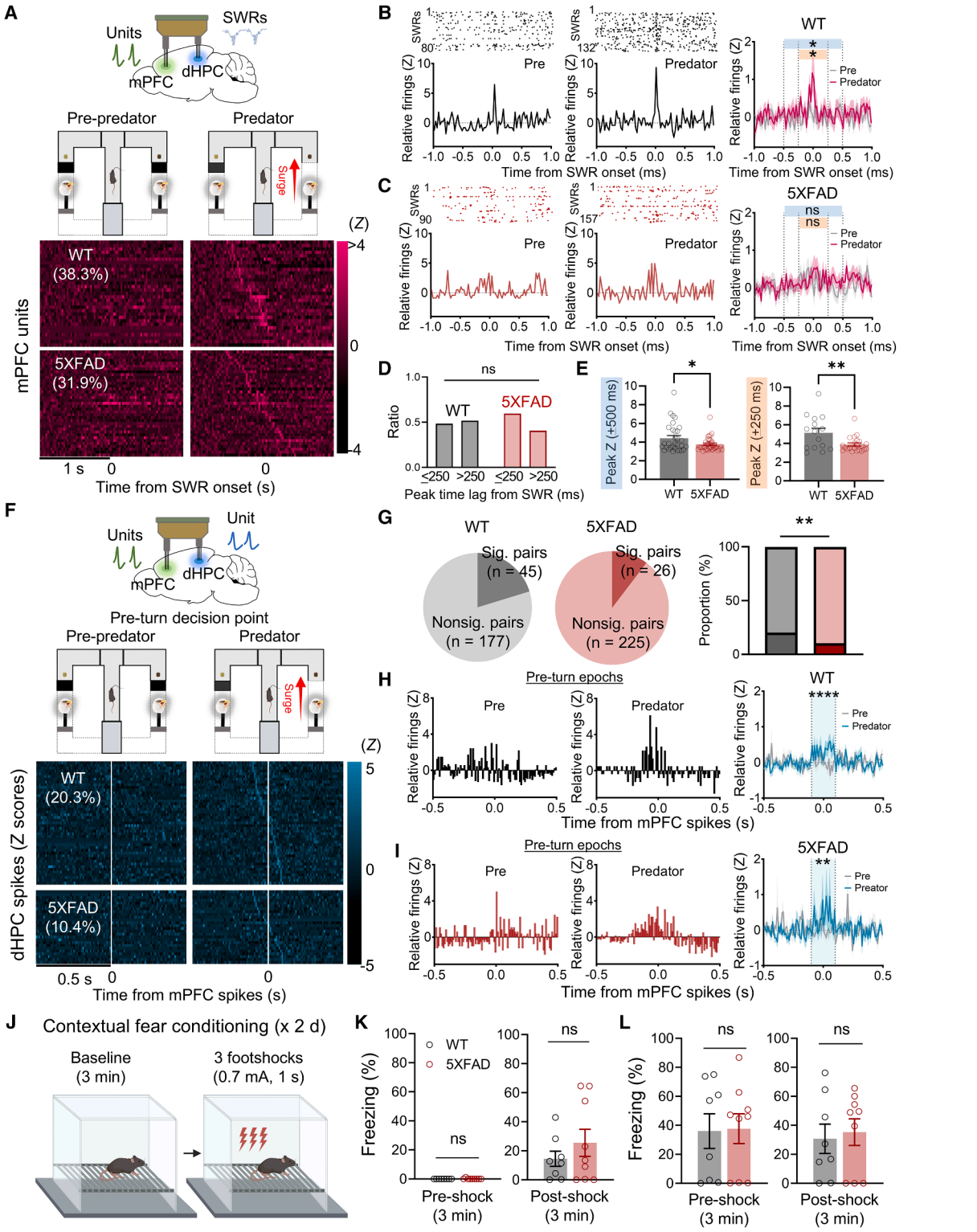


Figure 4. 5XFAD mice exhibit altered dHPC-mPFC interactions during foraging under predatory risk

(A) Top: dHPC SWR and unit activity analyzed during pre-predator and predator sessions. Bottom: color-coded activity (*Z* scores) of significantly firing mPFC units during peri-SWR epochs in predator trials, aligned with SWR onset for each session.

(legend continued on next page)

compared to pre-predator levels (Figures 3D–3G). However, key differences emerged in the temporal alignment of firing to SWRs; WT dHPC neurons exhibited peak firing closely aligned with SWR onset (Figure 3H), whereas 5XFAD dHPC neurons showed delayed peak firing (Figure S4B). Moreover, peak firing rates of dHPC cells during both time windows were significantly higher in WT mice (Figures 3I, S4C, and S4D). These results indicate disrupted SWR-spike coordination in 5XFAD mice, suggesting impaired dHPC synchronization during risky decision-making.

We next examined SWR activity and dHPC firing during a post-predator rest period in the nest (Figure S5A). Consistent with prior observations,[58,59] 5XFAD mice exhibited fewer (Figure S5B, left) and shorter (Figure S5C) dCA1 SWRs than WT mice. Movement speed did not differ between groups (Figure S5D), confirming that SWR frequency differences were not movement related. When categorized by behavioral state—moving (velocity $\geq$5 cm/s) vs. stationary (velocity <5 cm/s)—5XFAD mice showed a reduced SWR frequency in both states (Figure S5B, middle and right). Given that SWRs during movement and immobility have been linked to future planning and memory consolidation, respectively,[68–72] these reductions suggest broader disruptions in decision-relevant cognitive processes.

Analysis of peri-SWR dHPC activity (±250 ms window) revealed that WT mice had more SWR-modulated units and shorter SWR-firing lags than 5XFAD mice (Figures S5E and S5F). Peak firing relative to SWR onset was also delayed in 5XFAD mice (Figure S5G). However, maximal firing rates during the ±250 ms and ±100 ms periods were comparable between groups (Figure S5H). These findings suggest Aβ pathology disrupts SWR-associated dHPC firing coordination during post-threat processing.

Finally, we examined the relationship between amyloid burden and SWR activity. While dHPC Aβ plaque levels did not correlate with SWR frequency during the pre-predator session, we observed significant negative correlations during both predator and post-predator sessions (Figure S6, top). Additionally, mPFC Aβ levels were negatively correlated with SWR frequency during the post-predator session (Figure S6, bottom). Together, these findings identify SWR-associated hippocampal activity as a potential *in vivo* biomarker for AD-related dysfunction and highlight its relevance to cognitive impairments, particularly in risky decision-making contexts.

5XFAD mice exhibit altered dHPC-mPFC dynamics during foraging under predatory risks

To examine how Aβ pathology affects hippocampal-prefrontal interactions, we analyzed dHPC SWRs and their influence on mPFC firing during foraging under predatory risks (Figure 4A). Comparable proportions of mPFC neurons exhibited significant peri-SWR firing ($Z > 3$) during predator sessions in WT (38.3%) and 5XFAD (31.9%) mice. In WT mice, mPFC cells showed increased firing within ±500 and ±250 ms of SWR onset during predator compared to pre-predator sessions (Figures 4B, S7A, and S7B). This modulation was absent in 5XFAD mice, whose mean mPFC firing rates in response to SWRs did not differ between sessions (Figures 4C and S7C).

Although the proportion of mPFC cells with peak firing near SWR onset was similar across genotypes (Figure 4D), peak Z values during the ±500 ms and ±250 periods relative to SWR onset were significantly higher in WT mice (Figure 4E). These findings indicate that dHPC SWRs modulate mPFC activity in WT but not 5XFAD mice, suggesting impaired dHPC-mPFC coordination during risky decision-making in AD models.

To further assess decision-related dHPC-mPFC interactions, we examined spike synchrony in the "decision zone" before animals turned toward either the preferred (risky) or non-preferred (safe) arm (Figure 4F). Cross-correlograms (CCs) were computed using mPFC spikes as reference during 3-s pre-turn epochs for pre-predator and predator decision points. We recorded 1,060 dHPC-mPFC neuron pairs (WT. 462; 5XFAD, 598) across sessions and analyzed 222 WT and 251 5XFAD pairs with firing rates >0.2 Hz.

At predator decision points, a higher proportion of WT pairs (20.3%, 45 of 222) showed spike synchrony than 5XFAD pairs (10.4%, 26 of 251), indicating reduced dHPC-mPFC synchrony in 5XFAD mice (Figure 4G). Analysis of dHPC firing rates relative to mPFC spikes during the ±100 ms period revealed elevated mean and peak dHPC firing rates during predator vs. pre-predator sessions in both groups (Figures 4H, 4I, and S7D–S7F). However, reduced synchrony in 5XFAD mice highlights a breakdown in dHPC-mPFC functional coordination during risky decision-making.

Given these findings and prior work implicating theta rhythms in hippocampal-prefrontal interactions during decision-making, we examined theta (6–10 Hz)[44,73–75] dynamics during the 3-s pre-turn decision window. In WT mice, dHPC theta power

(B) Representative (left and middle) peri-SWR activity of WT mPFC neurons exhibiting significant activity ($Z > 3$) around SWR onset during the predator session. Right: group peri-SWR activity of WT mPFC neurons with significant activity ($Z > 3$) within the ±500 ms period around SWR onset during the predator session. Mean Z scores during the ±500 ms (blue) and ±250 ms (orange) periods were compared between sessions.
(C) Representative and group peri-SWR activity of 5XFAD mPFC neurons as in (B).
(D) Proportions of mPFC neurons exhibiting significant activity within the ±500 ms vs. ±250 ms periods in WT and 5XFAD mice.
(E) SWR-related mPFC cell activity (peak Z scores within the ±500 ms and ±250 ms periods) compared between WT and 5XFAD mice during the predator session.
(F) Analysis of dHPC-mPFC synchronous activity during pre-predator and predator sessions. Color-coded cross-correlograms (CCs) show significant dHPC-mPFC spike synchrony during 3-s pre-turn epochs before animals made turns in the presence of a predator.
(G) Proportion of significantly correlated dHPC-mPFC pairs in WT (left) and 5XFAD (middle) groups during the predator session; group comparison is shown (right).
(H and I) Representative (left and middle) and group (right) dHPC-mPFC CCs from WT (H) and 5XFAD (I) mice showing significant peaks (−100 to 100 ms, blue-shaded area) during pre-turn epochs with a predator present.
(J) Behavioral procedure for contextual fear conditioning.
(K and L) Freezing levels during pre-shock (3 min) and post-shock (3 min) phases on days 1 (K) and 2 (L) of contextual fear conditioning.
Data are presented as mean ± SEM. $^{*}p < 0.05$, $^{**}p < 0.01$, $^{****}p < 0.0001$. See also Figures S7–S9.

increased under predatory threat (Figure S8A), consistent with its role in guiding decision-making and processing emotional context.[44,76–78] This increase was absent in 5XFAD mice (Figure S8B), and the overall theta power ratio across sessions was significantly lower in 5XFAD mice across sessions (Figure S8C). In contrast, mPFC theta power did not differ significantly by genotype or threat level (Figures S8D–S8F).

To assess functional coupling, we analyzed phase-locking of mPFC units to dHPC theta oscillations during the 3-s pre-turn epoch (the decision window) (Figures S8G and S8H). The mean resultant length, a standard measure of phase-locking strength,[79,80] was comparable between WT (n = 31 neurons) and 5XFAD (n = 41 neurons) mice across both the pre-predator and predator sessions (Figure S8I). Due to the limited number of trials per session (pre-predator, 8–14; predator, 3–10), fewer cells met the inclusion criterion of >40 spikes[81–83] for phase-locking analysis. While the proportion of significantly phase-locked mPFC neurons ($p < 0.05$, Rayleigh test) did not differ between groups in the pre-predator session (Figure S8J), a greater percentage of WT mPFC neurons was phase-locked compared to 5XFAD neurons during the predator session (Figure S8K), indicating reduced theta-mediated dHPC-mPFC coordination in 5XFAD mice.

To rule out general deficits in fear learning, we assessed contextual fear conditioning following the predator task (Figure 4J). 5XFAD and WT mice exhibited similar post-shock and contextual freezing levels across days (Figures 4K, 4L, S9A, and S9B), suggesting intact fear learning and foot shock sensitivity. Thus, altered risky foraging in 5XFAD mice is not due to general impairment in aversive processing.

Taken together, 5XFAD mice exhibit reduced mPFC modulation by dHPC SWRs and diminished dHPC-mPFC synchrony and theta coupling during threat-based decision making. These disruptions in hippocampal-prefrontal dynamics may underlie impaired risk-based choices in AD and highlight a potential mechanistic link between Aβ pathology and decision-making deficits.

DISCUSSION

Using two distinct predatory threat scenarios and simultaneous mPFC-dHPC recordings, this study reveals cognitive and neural alterations in 5XFAD mice that mirror risky decision-making deficits observed in patients with AD.[5,8,22,84] Behaviorally, 5XFAD mice exhibited heightened risk-taking, marked by longer foraging distances and inflexible strategies, despite intact contextual fear conditioning and predator-evoked flight responses. This selective deficit, observed in both 4- to 5- and 7- to 9-month-old 5XFAD mice, supports the utility of ecologically relevant foraging paradigms in potentially detecting early-stage AD-related cognitive dysfunction.

At the neural level, risk-prone behavior in 5XFAD mice was accompanied by reduced dCA1 SWR frequency and disrupted mPFC-dHPC connectivity. SWRs are established "cognitive biomarkers" of memory consolidation, retrieval, and planning,[67,85,86] and their decline has been linked to aging[87,88] in AD mouse models.[58,55] Real-time interference with SWRs impairs memory,[54] while prolonging SWRs improves it,[89] underscoring their cognitive relevance. Our findings linking Aβ plaques with SWR activity and risky decision-making suggest that dysfunctional SWRs contribute to cognitive decline in 5XFAD mice. This aligns with prior work on SWR contributions to spatial memory, navigation, and decision-making under risk.[52,67,85,86,89,90]

Although 5XFAD and WT mice showed similar proportions of dHPC neurons firing during SWRs in predator sessions, 5XFAD hippocampal cells exhibited delayed peak firing relative to SWR onset, suggesting reduced temporal synchrony, a finding consistent with previous reports of weakened hippocampal co-activation during SWRs in AD mice.[59] This temporal misalignment may underlie inefficient hippocampal cell activity and contribute to impaired cognition.

mPFC-dHPC interactions, including coordinated replay, oscillatory coupling, and phase-locked firing, are critical for decision-making.[41,52,78] For instance, distinct CA1-mPFC replay patterns encode either past experiences or future decisions during spatial learning.[91,92] Oscillatory coupling between the hippocampus and mPFC occurs across multiple frequency bands, including theta, gamma, and SWRs, during goal-directed behavior.[80,93–98] Notably, mPFC neurons increase phase-locking to hippocampal theta oscillations during decision-making epochs[99–101] and anxiety-related behaviors.[102,103] In WT mice, predator exposure increased mPFC firing within 500 ms of SWR onset, a response absent in 5XFAD mice. This blunted mPFC reactivity, combined with reduced dHPC-mPFC synchrony at decision regions, points to disrupted circuit-level integration. Additional deficits in hippocampal theta power and mPFC theta phase-locking further support a breakdown in inter-regional coordination. Given the role of the mPFC in rule switching, adaptive action selection, and memory-guided decisions,[53,104,105] impaired dHPC-mPFC coordination likely underlies the inflexible foraging observed in 5XFAD mice. These findings suggest that strategies to restore hippocampal-prefrontal synchrony or enhance SWR activity via lifestyle interventions (e.g., exercise and diet)[106,107] or therapeutic approaches (e.g., pharmacological,[108] genetic,[109] neuromodulation,[110] or gut microbiome[111] interventions) may mitigate cognitive decline in AD.

Place cell coding properties in Aβ mouse models are variable. For example, while Tg2576 mice (16 months old) exhibit reduced spatial information and enlarged place fields,[112] 5XFAD mice (4–14 months old) show the opposite.[113] Place field stability also varies; APP KI (7–13 months old) and J20 APP (7 months old) mice retain stable maps in familiar contexts,[114,115] whereas 3xTg mice (8–9 months old, which develop both Aβ and tau pathology) show less stable place fields.[116] Aβ models also display experience-dependent coding deficits; APP-PS1 place cells fail to adapt to learned changes,[114,115] and APP KI mice struggle with remapping on a different track.[117] Here, we found rigid place cell firing in 5XFAD mice, particularly in predator-exposed zones. This inflexibility contrasts with WT mice (Figures 2H and 2I), which showed remapping not only in the threat zone but also across adjacent maze regions, suggesting that spatial representations in WT mice are shaped by internal states such as fear anticipation. In 5XFAD mice, by contrast, this integration of spatial and emotional information was impaired, revealing a potential mechanism for decision-making deficits.

Although 5XFAD mice showed intact contextual fear conditioning, a hippocampus-dependent task,[118,119] reduced innate fear could still influence foraging. Previous reports showed impaired contextual fear in older (>6 months) but not younger (<4 months) 5XFAD mice.[120] However, our data from 8- to 11-month-old animals showed no genotype differences, consistent with findings in APP-KI (12- to 13-month-old)[114] and Tg2575 (16- to 18-month-old) models.[121] It is possible that the standard fear conditioning, with limited chamber cues and aversive foot shocks, masks subtle hippocampal dysfunction. As Thorndike (1899) noted, animals may solve tasks in constrained environments through simple associations.[122] In contrast, naturalistic foraging tasks require complex spatial navigation and dynamic threat assessment, making them more sensitive to early AD-related changes.

In conclusion, these results collectively highlight the value of ecologically valid tasks in detecting risky decision-making and neural alterations in AD. In 5XFAD mice, Aβ pathology was associated with impaired risk-based foraging, reduced SWR activity, disrupted place coding, and weakened mPFC-dHPC coordination. As decision-making deficits may precede memory loss in clinical settings, ecological behavioral assays and network-level analyses could serve as sensitive tools for early detection, mechanistic insights, and targeted intervention development. Future studies should explore strategies to enhance SWR activity and cortico-hippocampal coordination as potential avenues to slow or reverse cognitive decline in AD.

Limitations of the study

First, while prior studies[113,114] report general spatial inflexibility in AD models, our findings suggest more specific threat-related remapping deficits. In our task, the predator was visible only in the distal zone, yet WT mice exhibited remapping across broader maze regions (e.g., the center arm). This indicates that internal states, such as fear or vigilance, modulated spatial coding in WT but not in 5XFAD mice. Future work using neutral or non-aversive manipulations could clarify whether the observed remapping deficits reflect global spatial inflexibility or a specific disruption in threat-modulated coding. Second, decision-making impairments in 5XFAD mice may stem from broader cortico-limbic dysfunction beyond the dHPC-mPFC circuit. The amygdala and ventral hippocampus, both affected in AD,[123–126] are critical for emotion, salience, and risk evaluation.[43,66,102,103,127] Future studies should examine whether these regions also contribute to disrupted dHPC-mPFC interactions and risk-related decision-making in AD.

RESOURCE AVAILABILITY

Lead contact

Requests for further information and resources should be directed to the lead contact, Jeansok J. Kim (jeansokk@uw.edu).

Materials availability

This study did not generate new unique reagents.

Data and code availability

- All data are available from the lead contact upon request.
- Code is publicly available at GitHub: https://github.com/KimLab-UW-NSB/5xfad-hpc-pfc-neural-dynamics.git.
- Additional details to reproduce analyses are available upon request.

ACKNOWLEDGMENTS

This study was supported by NIH grants AG067008 (to E.J.K.), MH139585 (to J.J.K.), UW Royalty Research Fund A188443 (to E.J.K.), National Research Foundation of Korea RS-2025-00522887 (to J.C.), and ETRI 25YB1210 (to S.P.). We thank Drs. Min Whan Jung and Jong Won Lee (Korea Advanced Institute of Science and Technology) for generously sharing custom-made microdrive components and electronic interface boards and Nayoung Kim for assistance with experiments and data collection/analysis. Illustrations were created with BioRender.

AUTHOR CONTRIBUTIONS

E.J.K., J.C., and J.J.K. conceived and designed the research. E.J.K., S.P., B.P.S., and H.B. conducted behavioral and neurophysiological experiments and analyses. E.J.K., S.P., J.C., and J.J.K. wrote and edited the manuscript.

DECLARATION OF INTERESTS

The authors declare no competing interests.

STAR★METHODS

Detailed methods are provided in the online version of this paper and include the following:

- KEY RESOURCES TABLE
- EXPERIMENTAL MODEL AND STUDY PARTICIPANT DETAILS
  - Animals
- METHOD DETAILS
  - Surgery
  - Escalating predatory risk
  - Conditional predatory risk
  - Contextual fear conditioning
  - Electrophysiological recording and analysis
  - Histology
- QUANTIFICATION AND STATISTICAL ANALYSIS
  - Statistical analyses analysis

SUPPLEMENTAL INFORMATION

Supplemental information can be found online at https://doi.org/10.1016/j.celrep.2025.116081.

Received: December 23, 2024
Revised: June 5, 2025
Accepted: July 10, 2025
Published: July 29, 2025

REFERENCES

1. Bangma, D.F., Tucha, O., Tucha, L., De Deyn, P.P., and Koerts, J. (2021). How well do people living with neurodegenerative diseases manage their finances? A meta-analysis and systematic review on the capacity to make financial decisions in people living with neurodegenerative diseases. Neurosci. Biobehav. Rev. *127*, 709–739. https://doi.org/10.1016/j.neubiorev.2021.05.021.
2. Bertrand, E., van Duinkerken, E., Landeira-Fernandez, J., Dourado, M.C. N., Santos, R.L., Laks, J., and Mograbi, D.C. (2017). Behavioral and Psychological Symptoms Impact Clinical Competence in Alzheimer's Disease. Front. Aging Neurosci. *9*, 182. https://doi.org/10.3389/fnagi.2017.00182.

3. Delazer, M., Sinz, H., Zamarian, L., and Benke, T. (2007). Decision-making with explicit and stable rules in mild Alzheimer's disease. Neuropsychologia *45*, 1632–1641. https://doi.org/10.1016/j.neuropsychologia.2007.01.006.

4. Gleichgerrcht, E., Ibáñez, A., Roca, M., Torralva, T., and Manes, F. (2010). Decision-making cognition in neurodegenerative diseases. Nat. Rev. Neurol. *6*, 611–623. https://doi.org/10.1038/nrneurol.2010.148.

5. Ha, J., Kim, E.J., Lim, S., Shin, D.W., Kang, Y.J., Bae, S.M., Yoon, H.K., and Oh, K.S. (2012). Altered risk-aversion and risk-taking behaviour in patients with Alzheimer's disease. Psychogeriatrics *12*, 151–158. https://doi.org/10.1111/j.1479-8301.2011.00396.x.

6. Marson, D.C., Martin, R.C., Wadley, V., Griffith, H.R., Snyder, S., Goode, P.S., Kinney, F.C., Nicholas, A.P., Steele, T., Anderson, B., et al. (2009). Clinical interview assessment of financial capacity in older adults with mild cognitive impairment and Alzheimer's disease. J. Am. Geriatr. Soc. *57*, 806–814. https://doi.org/10.1111/j.1532-5415.2009.02202.x.

7. Okonkwo, O., Griffith, H.R., Belue, K., Lanza, S., Zamrini, E.Y., Harrell, L. E., Brockington, J.C., Clark, D., Raman, R., and Marson, D.C. (2007). Medical decision-making capacity in patients with mild cognitive impairment. Neurology *69*, 1528–1535. https://doi.org/10.1212/01.wnl.0000277639.90611.d9.

8. Sun, T., Xie, T., Wang, J., Zhang, L., Tian, Y., Wang, K., Yu, X., and Wang, H. (2020). Decision-Making Under Ambiguity or Risk in Individuals With Alzheimer's Disease and Mild Cognitive Impairment. Front. Psychiatry *11*, 218. https://doi.org/10.3389/fpsyt.2020.00218.

9. Sun, W., Matsuoka, T., and Narumoto, J. (2021). Decision-Making Support for People With Alzheimer's Disease: A Narrative Review. Front. Psychol. *12*, 750803. https://doi.org/10.3389/fpsyg.2021.750803.

10. van Duinkerken, E., Farme, J., Landeira-Fernandez, J., Dourado, M.C., Laks, J., and Mograbi, D.C. (2018). Medical and Research Consent Decision-Making Capacity in Patients with Alzheimer's Disease: A Systematic Review. J. Alzheimers Dis. *65*, 917–930. https://doi.org/10.3233/JAD-180311.

11. Boyle, P.A., Yu, L., Schneider, J.A., Wilson, R.S., and Bennett, D.A. (2019). Scam Awareness Related to Incident Alzheimer Dementia and Mild Cognitive Impairment: A Prospective Cohort Study. Ann. Intern. Med. *170*, 702–709. https://doi.org/10.7326/M18-2711.

12. Davis, R., Ziomkowski, M.K., and Veltkamp, A. (2017). Everyday Decision Making in Individuals with Early-Stage Alzheimer's Disease: An Integrative Review of the Literature. Res. Gerontol. Nurs. *10*, 240–247. https://doi.org/10.3928/19404921-20170831-05.

13. Gerstenecker, A., Triebel, K.L., Martin, R., Snyder, S., and Marson, D.C. (2016). Both Financial and Cognitive Decline Predict Clinical Progression in MCI. Alzheimer Dis. Assoc. Disord. *30*, 27–34. https://doi.org/10.1097/WAD.0000000000000120.

14. Han, S.D., Boyle, P.A., James, B.D., Yu, L., and Bennett, D.A. (2015). Mild cognitive impairment is associated with poorer decision-making in community-based older persons. J. Am. Geriatr. Soc. *63*, 676–683. https://doi.org/10.1111/jgs.13346.

15. Martin, R.C., Gerstenecker, A., Triebel, K.L., Falola, M., McPherson, T., Cutter, G., and Marson, D.C. (2019). Declining Financial Capacity in Mild Cognitive Impairment: A Six-Year Longitudinal Study. Arch. Clin. Neuropsychol. *34*, 152–161. https://doi.org/10.1093/arclin/acy030.

16. Niccolai, L.M., Triebel, K.L., Gerstenecker, A., McPherson, T.O., Cutter, G.R., Martin, R.C., and Marson, D.C. (2017). Neurocognitive Predictors of Declining Financial Capacity in Persons with Mild Cognitive Impairment. Clin. Gerontol. *40*, 14–23. https://doi.org/10.1080/07317115.2016.1228022.

17. Okonkwo, O.C., Griffith, H.R., Copeland, J.N., Belue, K., Lanza, S., Zamrini, E.Y., Harrell, L.E., Brockington, J.C., Clark, D., Raman, R., and Marson, D.C. (2008). Medical decision-making capacity in mild cognitive impairment: a 3-year longitudinal study. Neurology *71*, 1474–1480. https://doi.org/10.1212/01.wnl.0000334301.32358.48.

18. Spreng, R.N., PhD, Karlawish, J., Md, and Marson, D.C., Md. (2016). Cognitive, social, and neural determinants of diminished decision-making and financial exploitation risk in aging and dementia: A review and new model. J. Elder Abuse Negl. *28*, 320–344. https://doi.org/10.1080/08946566.2016.1237918.

19. Triebel, K.L., Martin, R., Griffith, H.R., Marceaux, J., Okonkwo, O.C., Harrell, L., Clark, D., Brockington, J., Bartolucci, A., and Marson, D.C. (2009). Declining financial capacity in mild cognitive impairment: A 1-year longitudinal study. Neurology *73*, 928–934. https://doi.org/10.1212/WNL.0b013e3181b87971.

20. Yerstein, O., Carr, A.R., Jimenez, E., and Mendez, M.F. (2020). Neuropsychiatric Effects on Decision-Making in Early Alzheimer Disease. J. Geriatr. Psychiatry Neurol. *33*, 68–72. https://doi.org/10.1177/0891988719888292.

21. Kapasi, A., Yu, L., Stewart, C., Schneider, J.A., Bennett, D.A., and Boyle, P.A. (2021). Association of Amyloid-beta Pathology with Decision Making and Scam Susceptibility. J. Alzheimers Dis. *83*, 879–887. https://doi.org/10.3233/JAD-210356.

22. Sinz, H., Zamarian, L., Benke, T., Wenning, G.K., and Delazer, M. (2008). Impact of ambiguity and risk on decision making in mild Alzheimer's disease. Neuropsychologia *46*, 2043–2055. https://doi.org/10.1016/j.neuropsychologia.2008.02.002.

23. Grossberg, S., and Gutowski, W.E. (1987). Neural dynamics of decision making under risk: affective balance and cognitive-emotional interactions. Psychol. Rev. *94*, 300–318.

24. Heilman, R.M., Crişan, L.G., Houser, D., Miclea, M., and Miu, A.C. (2010). Emotion regulation and decision making under risk and uncertainty. Emotion *10*, 257–265. https://doi.org/10.1037/a0018489.

25. Wang, Y., and Ruhe, G. (2007). The cognitive process of decision making. Int. J. Cognit. Inf. Nat. Intell. *1*, 73–85.

26. Anderson, R., Hart, D.W., Sweis, B., Sherman, M.A., Thomas, M.J., Redish, A.D., and Lesné, S.E. (2021). Sex-specific interactions between procedural and deliberative decision-making systems in a mouse model of Alzheimer's disease. Preprint at: bioRxiv. https://doi.org/10.1101/2021.03.16.435712

27. Bateman, R.J., Smith, J., Donohue, M.C., Delmar, P., Abbas, R., Salloway, S., Wojtowicz, J., Blennow, K., Bittner, T., Black, S.E., et al. (2023). Two Phase 3 Trials of Gantenerumab in Early Alzheimer's Disease. N. Engl. J. Med. *389*, 1862–1876. https://doi.org/10.1056/NEJMoa2304430.

28. Cacabelos, R. (2018). Have there been improvements in Alzheimer's disease drug discovery over the past 5 years? Expert Opin. Drug Discov. *13*, 523–538. https://doi.org/10.1080/17460441.2018.1457645.

29. Mehta, D., Jackson, R., Paul, G., Shi, J., and Sabbagh, M. (2017). Why do trials for Alzheimer's disease drugs keep failing? A discontinued drug perspective for 2010-2015. Expert Opin. Investig. Drugs *26*, 735–739. https://doi.org/10.1080/13543784.2017.1323868.

30. Driscoll, I., and Troncoso, J. (2011). Asymptomatic Alzheimer's disease: a prodrome or a state of resilience? Curr. Alzheimer Res. *8*, 330–335. https://doi.org/10.2174/156720511795745348.

31. Hohman, T.J., McLaren, D.G., Mormino, E.C., Gifford, K.A., Libon, D.J., and Jefferson, A.L.; Alzheimer's Disease Neuroimaging Initiative (2016). Asymptomatic Alzheimer disease: Defining resilience. Neurology *87*, 2443–2450. https://doi.org/10.1212/WNL.0000000000003397.

32. Latimer, C.S., Keene, C.D., Flanagan, M.E., Hemmy, L.S., Lim, K.O., White, L.R., Montine, K.S., and Montine, T.J. (2017). Resistance to Alzheimer Disease Neuropathologic Changes and Apparent Cognitive Resilience in the Nun and Honolulu-Asia Aging Studies. J. Neuropathol. Exp. Neurol. *76*, 458–466. https://doi.org/10.1093/jnen/nlx030.

33. Boyle, R., Klinger, H.M., Shirzadi, Z., Coughlan, G.T., Seto, M., Properzi, M.J., Townsend, D.L., Yuan, Z., Scanlon, C., Jutten, R.J., et al. (2024). Left Frontoparietal Control Network Connectivity Moderates the Effect of Amyloid on Cognitive Decline in Preclinical Alzheimer's Disease: The

A4 Study. J. Prev. Alzheimers Dis. *11*, 881–888. https://doi.org/10.14283/jpad.2024.140.

34. Buckley, R.F., Schultz, A.P., Hedden, T., Papp, K.V., Hanseeuw, B.J., Marshall, G., Sepulcre, J., Smith, E.E., Rentz, D.M., Johnson, K.A., et al. (2017). Functional network integrity presages cognitive decline in preclinical Alzheimer disease. Neurology *89*, 29–37. https://doi.org/10.1212/WNL.0000000000004059.
35. Walsh, C., Drinkenburg, W.H.I.M., and Ahnaou, A. (2017). Neurophysiological assessment of neural network plasticity and connectivity: Progress towards early functional biomarkers for disease interception therapies in Alzheimer's disease. Neurosci. Biobehav. Rev. *73*, 340–358. https://doi.org/10.1016/j.neubiorev.2016.12.020.
36. Corcoran, K.A., and Maren, S. (2001). Hippocampal inactivation disrupts contextual retrieval of fear memory after extinction. J. Neurosci. *21*, 1720–1726.
37. Corcoran, K.A., and Quirk, G.J. (2007). Activity in prelimbic cortex is necessary for the expression of learned, but not innate, fears. J. Neurosci. *27*, 840–844. https://doi.org/10.1523/JNEUROSCI.5327-06.2007.
38. Gluth, S., Sommer, T., Rieskamp, J., and Büchel, C. (2015). Effective Connectivity between Hippocampus and Ventromedial Prefrontal Cortex Controls Preferential Choices from Memory. Neuron *86*, 1078–1090. https://doi.org/10.1016/j.neuron.2015.04.023.
39. Rhodes, S.E.V., and Murray, E.A. (2013). Differential effects of amygdala, orbital prefrontal cortex, and prelimbic cortex lesions on goal-directed behavior in rhesus macaques. J. Neurosci. *33*, 3380–3389. https://doi.org/10.1523/JNEUROSCI.4374-12.2013.
40. Yoon, T., Okada, J., Jung, M.W., and Kim, J.J. (2008). Prefrontal cortex and hippocampus subserve different components of working memory in rats. Learn. Mem. *15*, 97–105. https://doi.org/10.1101/lm.850808.
41. Yu, J.Y., and Frank, L.M. (2015). Hippocampal-cortical interaction in decision making. Neurobiol. Learn. Mem. *117*, 34–41. https://doi.org/10.1016/j.nlm.2014.02.002.
42. Euston, D.R., Gruber, A.J., and McNaughton, B.L. (2012). The role of medial prefrontal cortex in memory and decision making. Neuron *76*, 1057–1070. https://doi.org/10.1016/j.neuron.2012.12.002.
43. Kim, E.J., Kong, M.S., Park, S.G., Mizumori, S.J.Y., Cho, J., and Kim, J.J. (2018). Dynamic coding of predatory information between the prelimbic cortex and lateral amygdala in foraging rats. Sci. Adv. *4*, eaar7328. https://doi.org/10.1126/sciadv.aar7328.
44. Kim, E.J., Park, M., Kong, M.S., Park, S.G., Cho, J., and Kim, J.J. (2015). Alterations of hippocampal place cells in foraging rats facing a "predatory" threat. Curr. Biol. *25*, 1362–1367. https://doi.org/10.1016/j.cub.2015.03.048.
45. Bayard, S., Jacus, J.P., Raffard, S., and Gely-Nargeot, M.C. (2014). Apathy and emotion-based decision-making in amnesic mild cognitive impairment and Alzheimer's disease. Behav. Neurol. *2014*, 231469. https://doi.org/10.1155/2014/231469.
46. Eimer, W.A., and Vassar, R. (2013). Neuron loss in the 5XFAD mouse model of Alzheimer's disease correlates with intraneuronal Abeta42 accumulation and Caspase-3 activation. Mol. Neurodegener. *8*, 2. https://doi.org/10.1186/1750-1326-8-2.
47. Oakley, H., Cole, S.L., Logan, S., Maus, E., Shao, P., Craft, J., Guillozet-Bongaarts, A., Ohno, M., Disterhoft, J., Van Eldik, L., et al. (2006). Intraneuronal beta-amyloid aggregates, neurodegeneration, and neuron loss in transgenic mice with five familial Alzheimer's disease mutations: potential factors in amyloid plaque formation. J. Neurosci. *26*, 10129–10140. https://doi.org/10.1523/JNEUROSCI.1202-06.2006.
48. Girard, S.D., Baranger, K., Gauthier, C., Jacquet, M., Bernard, A., Escoffier, G., Marchetti, E., Khrestchatisky, M., Rivera, S., and Roman, F.S. (2013). Evidence for early cognitive impairment related to frontal cortex in the 5XFAD mouse model of Alzheimer's disease. J. Alzheimers Dis. *33*, 781–796. https://doi.org/10.3233/JAD-2012-120982.
49. Sadleir, K.R., Popovic, J., and Vassar, R. (2018). ER stress is not elevated in the 5XFAD mouse model of Alzheimer's disease. J. Biol. Chem. *293*, 18434–18443. https://doi.org/10.1074/jbc.RA118.005769.
50. Girardeau, G., Inema, I., and Buzsáki, G. (2017). Reactivations of emotional memory in the hippocampus-amygdala system during sleep. Nat. Neurosci. *20*, 1634–1642. https://doi.org/10.1038/nn.4637.
51. Schmidt, B., and Redish, A.D. (2021). Disrupting the medial prefrontal cortex with designer receptors exclusively activated by designer drug alters hippocampal sharp-wave ripples and their associated cognitive processes. Hippocampus *31*, 1051–1067. https://doi.org/10.1002/hipo.23367.
52. Colgin, L.L. (2011). Oscillations and hippocampal-prefrontal synchrony. Curr. Opin. Neurobiol. *21*, 467–474. https://doi.org/10.1016/j.conb.2011.04.006.
53. den Bakker, H., Van Dijck, M., Sun, J.J., and Kloosterman, F. (2023). Sharp-wave-ripple-associated activity in the medial prefrontal cortex supports spatial rule switching. Cell Rep. *42*, 112959. https://doi.org/10.1016/j.celrep.2023.112959.
54. Jadhav, S.P., Rothschild, G., Roumis, D.K., and Frank, L.M. (2016). Coordinated Excitation and Inhibition of Prefrontal Ensembles during Awake Hippocampal Sharp-Wave Ripple Events. Neuron *90*, 113–127. https://doi.org/10.1016/j.neuron.2016.02.010.
55. Jura, B., Macrez, N., Meyrand, P., and Bem, T. (2019). Deficit in hippocampal ripples does not preclude spatial memory formation in APP/PS1 mice. Sci. Rep. *9*, 20129. https://doi.org/10.1038/s41598-019-56582-w.
56. Gillespie, A.K., Jones, E.A., Lin, Y.H., Karlsson, M.P., Kay, K., Yoon, S.Y., Tong, L.M., Nova, P., Carr, J.S., Frank, L.M., and Huang, Y. (2016). Apolipoprotein E4 Causes Age-Dependent Disruption of Slow Gamma Oscillations during Hippocampal Sharp-Wave Ripples. Neuron *90*, 740–751. https://doi.org/10.1016/j.neuron.2016.04.009.
57. Jones, E.A., Gillespie, A.K., Yoon, S.Y., Frank, L.M., and Huang, Y. (2019). Early Hippocampal Sharp-Wave Ripple Deficits Predict Later Learning and Memory Impairments in an Alzheimer's Disease Mouse Model. Cell Rep. *29*, 2123–2133.e4. https://doi.org/10.1016/j.celrep.2019.10.056.
58. Iaccarino, H.F., Singer, A.C., Martorell, A.J., Rudenko, A., Gao, F., Gillingham, T.Z., Mathys, H., Seo, J., Kritskiy, O., Abdurrob, F., et al. (2016). Gamma frequency entrainment attenuates amyloid load and modifies microglia. Nature *540*, 230–235. https://doi.org/10.1038/nature20587.
59. Prince, S.M., Paulson, A.L., Jeong, N., Zhang, L., Amigues, S., and Singer, A.C. (2021). Alzheimer's pathology causes impaired inhibitory connections and reactivation of spatial codes during spatial navigation. Cell Rep. *35*, 109008. https://doi.org/10.1016/j.celrep.2021.109008.
60. Krakauer, J.W., Ghazanfar, A.A., Gomez-Marin, A., MacIver, M.A., and Poeppel, D. (2017). Neuroscience Needs Behavior: Correcting a Reductionist Bias. Neuron *93*, 480–490. https://doi.org/10.1016/j.neuron.2016.12.041.
61. Kempermann, G., Kuhn, H.G., and Gage, F.H. (1997). More hippocampal neurons in adult mice living in an enriched environment. Nature *386*, 493–495. https://doi.org/10.1038/386493a0.
62. Bennett, E.L., Diamond, M.C., Krech, D., and Rosenzweig, M.R. (1964). Chemical and Anatomical Plasticity Brain. Science *146*, 610–619. https://doi.org/10.1126/science.146.3644.610.
63. Pellman, B.A., and Kim, J.J. (2016). What Can Ethobehavioral Studies Tell Us about the Brain's Fear System? Trends Neurosci. *39*, 420–431. https://doi.org/10.1016/j.tins.2016.04.001.
64. Choi, J.S., and Kim, J.J. (2010). Amygdala regulates risk of predation in rats foraging in a dynamic fear environment. Proc. Natl. Acad. Sci. USA *107*, 21773–21777. https://doi.org/10.1073/pnas.1010079108.
65. Kim, J.J., Choi, J.-S., and Lee, H.J. (2016). Foraging in the face of fear: novel strategies for evaluating amygdala functions in rats. In Living

without an Amygdala, D.G. Amaral and R. Adolphs, eds. (The Guilford Press).

66. Kong, M.S., Kim, E.J., Park, S., Zweifel, L.S., Huh, Y., Cho, J., and Kim, J. J. (2021). Fearful-place' coding in the amygdala-hippocampal network. eLife *10*, e72040. https://doi.org/10.7554/eLife.72040.
67. Joo, H.R., and Frank, L.M. (2018). The hippocampal sharp wave-ripple in memory retrieval for immediate use and consolidation. Nat. Rev. Neurosci. *19*, 744–757. https://doi.org/10.1038/s41583-018-0077-1.
68. Diba, K., and Buzsáki, G. (2007). Forward and reverse hippocampal place-cell sequences during ripples. Nat. Neurosci. *10*, 1241–1242. https://doi.org/10.1038/nn1961.
69. Gillespie, A.K., Astudillo Maya, D.A., Denovellis, E.L., Liu, D.F., Kastner, D.B., Coulter, M.E., Roumis, D.K., Eden, U.T., and Frank, L.M. (2021). Hippocampal replay reflects specific past experiences rather than a plan for subsequent choice. Neuron *109*, 3149–3163.e6. https://doi.org/10.1016/j.neuron.2021.07.029.
70. Jadhav, S.P., Kemere, C., German, P.W., and Frank, L.M. (2012). Awake hippocampal sharp-wave ripples support spatial memory. Science *336*, 1454–1458. https://doi.org/10.1126/science.1217230.
71. Krause, E.L., and Drugowitsch, J. (2022). A large majority of awake hippocampal sharp-wave ripples feature spatial trajectories with momentum. Neuron *110*, 722–733.e8. https://doi.org/10.1016/j.neuron.2021.11.014.
72. Pfeiffer, B.E., and Foster, D.J. (2013). Hippocampal place-cell sequences depict future paths to remembered goals. Nature *497*, 74–79. https://doi.org/10.1038/nature12112.
73. Gray, J.A. (1978). The neuropsychology of anxiety. Br. J. Psychol. *69*, 417–434. https://doi.org/10.1111/j.2044-8295.1978.tb02118.x.
74. Monaco, J.D., Knierim, J.J., and Zhang, K. (2011). Sensory feedback, error correction, and remapping in a multiple oscillator model of place-cell activity. Front. Comput. Neurosci. *5*, 39. https://doi.org/10.3389/fncom.2011.00039.
75. Wikenheiser, A.M., and Redish, A.D. (2015). Hippocampal theta sequences reflect current goals. Nat. Neurosci. *18*, 289–294. https://doi.org/10.1038/nn.3909.
76. Belchior, H., Lopes-Dos-Santos, V., Tort, A.B.L., and Ribeiro, S. (2014). Increase in hippocampal theta oscillations during spatial decision making. Hippocampus *24*, 693–702. https://doi.org/10.1002/hipo.22260.
77. Seidenbecher, T., Laxmi, T.R., Stork, O., and Pape, H.C. (2003). Amygdalar and hippocampal theta rhythm synchronization during fear memory retrieval. Science *301*, 846–850. https://doi.org/10.1126/science.1085818.
78. Tang, W., Shin, J.D., and Jadhav, S.P. (2021). Multiple time-scales of decision-making in the hippocampus and prefrontal cortex. eLife *10*, e66227. https://doi.org/10.7554/eLife.66227.
79. Siapas, A.G., Lubenov, E.V., and Wilson, M.A. (2005). Prefrontal phase locking to hippocampal theta oscillations. Neuron *46*, 141–151. https://doi.org/10.1016/j.neuron.2005.02.028.
80. Sigurdsson, T., Stark, K.L., Karayiorgou, M., Gogos, J.A., and Gordon, J.A. (2010). Impaired hippocampal-prefrontal synchrony in a genetic mouse model of schizophrenia. Nature *464*, 763–767. https://doi.org/10.1038/nature08855.
81. Li, M., Wang, X., Yao, X., Wang, X., Chen, F., Zhang, X., Sun, S., He, F., Jia, Q., Guo, M., et al. (2021). Roles of Motor Cortex Neuron Classes in Reach-Related Modulation for Hemiparkinsonian Rats. Front. Neurosci. *15*, 645849. https://doi.org/10.3389/fnins.2021.645849.
82. van Wingerden, M., Vinck, M., Lankelma, J., and Pennartz, C.M.A. (2010). Theta-band phase locking of orbitofrontal neurons during reward expectancy. J. Neurosci. *30*, 7078–7087. https://doi.org/10.1523/JNEUROSCI.3860-09.2010.
83. Wang, Y., Liu, N., Ma, L., Yue, L., Cui, S., Liu, F.Y., Yi, M., and Wan, Y. (2024). Ventral Hippocampal CA1 Pyramidal Neurons Encode Nociceptive Information. Neurosci. Bull. *40*, 201–217. https://doi.org/10.1007/s12264-023-01086-x.
84. Gorrie, C.A., Brown, J., and Waite, P.M.E. (2008). Crash characteristics of older pedestrian fatalities: dementia pathology may be related to 'at risk' traffic situations. Accid. Anal. Prev. *40*, 912–919. https://doi.org/10.1016/j.aap.2007.10.006.
85. Buzsaki, G. (2015). Hippocampal sharp wave-ripple: A cognitive biomarker for episodic memory and planning. Hippocampus *25*, 1073–1188. https://doi.org/10.1002/hipo.22488.
86. Norman, Y., Yeagle, E.M., Khuvis, S., Harel, M., Mehta, A.D., and Malach, R. (2019). Hippocampal sharp-wave ripples linked to visual episodic recollection in humans. Science *365*, eaax1030. https://doi.org/10.1126/science.aax1030.
87. Cowen, S.L., Gray, D.T., Wiegand, J.P.L., Schimanski, L.A., and Barnes, C.A. (2020). Age-associated changes in waking hippocampal sharp-wave ripples. Hippocampus *30*, 28–38. https://doi.org/10.1002/hipo.23005.
88. Wiegand, J.P.L., Gray, D.T., Schimanski, L.A., Lipa, P., Barnes, C.A., and Cowen, S.L. (2016). Age Is Associated with Reduced Sharp-Wave Ripple Frequency and Altered Patterns of Neuronal Variability. J. Neurosci. *36*, 5650–5660. https://doi.org/10.1523/JNEUROSCI.3069-15.2016.
89. Fernandez-Ruiz, A., Oliva, A., Fermino de Oliveira, E., Rocha-Almeida, F., Tingley, D., and Buzsaki, G. (2019). Long-duration hippocampal sharp wave ripples improve memory. Science *364*, 1082–1086. https://doi.org/10.1126/science.aax0758.
90. Papale, A.E., Zielinski, M.C., Frank, L.M., Jadhav, S.P., and Redish, A.D. (2016). Interplay between Hippocampal Sharp-Wave-Ripple Events and Vicarious Trial and Error Behaviors in Decision Making. Neuron *92*, 975–982. https://doi.org/10.1016/j.neuron.2016.10.028.
91. Shin, J.D., Tang, W., and Jadhav, S.P. (2019). Dynamics of Awake Hippocampal-Prefrontal Replay for Spatial Learning and Memory-Guided Decision Making. Neuron *104*, 1110–1125.e7. https://doi.org/10.1016/j.neuron.2019.09.012.
92. Zielinski, M.C., Tang, W., and Jadhav, S.P. (2020). The role of replay and theta sequences in mediating hippocampal-prefrontal interactions for memory and cognition. Hippocampus *30*, 60–72. https://doi.org/10.1002/hipo.22821.
93. Bragin, A., Jandó, G., Nádasdy, Z., Hetke, J., Wise, K., and Buzsáki, G. (1995). Gamma (40-100 Hz) oscillation in the hippocampus of the behaving rat. J. Neurosci. *15*, 47–60. https://doi.org/10.1523/JNEUROSCI.15-01-00047.1995.
94. Remondes, M., and Wilson, M.A. (2013). Cingulate-hippocampus coherence and trajectory coding in a sequential choice task. Neuron *80*, 1277–1289. https://doi.org/10.1016/j.neuron.2013.08.037.
95. Shin, J.D., and Jadhav, S.P. (2016). Multiple modes of hippocampal-prefrontal interactions in memory-guided behavior. Curr. Opin. Neurobiol. *40*, 161–169. https://doi.org/10.1016/j.conb.2016.07.015.
96. Sirota, A., Montgomery, S., Fujisawa, S., Isomura, Y., Zugaro, M., and Buzsáki, G. (2008). Entrainment of neocortical neurons and gamma oscillations by the hippocampal theta rhythm. Neuron *60*, 683–697. https://doi.org/10.1016/j.neuron.2008.09.014.
97. Tavares, L.C.S., and Tort, A.B.L. (2022). Hippocampal-prefrontal interactions during spatial decision-making. Hippocampus *32*, 38–54. https://doi.org/10.1002/hipo.23394.
98. Weilbacher, R.A., and Gluth, S. (2016). The Interplay of Hippocampus and Ventromedial Prefrontal Cortex in Memory-Based Decision Making. Brain Sci. *7*. https://doi.org/10.3390/brainsci7010004.
99. Benchenane, K., Peyrache, A., Khamassi, M., Tierney, P.L., Gioanni, Y., Battaglia, F.P., and Wiener, S.I. (2010). Coherent theta oscillations and reorganization of spike timing in the hippocampal- prefrontal network upon learning. Neuron *66*, 921–936. https://doi.org/10.1016/j.neuron.2010.05.013.

100. Chen, C., Kim, J.J., Thompson, R.F., and Tonegawa, S. (1996). Hippocampal lesions impair contextual fear conditioning in two strains of mice. Behav. Neurosci. *110*, 1177–1180.

101. Jones, M.W., and Wilson, M.A. (2005). Theta rhythms coordinate hippocampal-prefrontal interactions in a spatial memory task. PLoS Biol. *3*, e402. https://doi.org/10.1371/journal.pbio.0030402.

102. Adhikari, A., Topiwala, M.A., and Gordon, J.A. (2010). Synchronized activity between the ventral hippocampus and the medial prefrontal cortex during anxiety. Neuron *65*, 257–269. https://doi.org/10.1016/j.neuron.2009.12.002.

103. Padilla-Coreano, N., Bolkan, S.S., Pierce, G.M., Blackman, D.R., Hardin, W.D., Garcia-Garcia, A.L., Spellman, T.J., and Gordon, J.A. (2016). Direct Ventral Hippocampal-Prefrontal Input Is Required for Anxiety-Related Neural Activity and Behavior. Neuron *89*, 857–866. https://doi.org/10.1016/j.neuron.2016.01.011.

104. Jarovi, J., Pilkiw, M., and Takehara-Nishiuchi, K. (2023). Prefrontal neuronal ensembles link prior knowledge with novel actions during flexible action selection. Cell Rep. *42*, 113492. https://doi.org/10.1016/j.celrep.2023.113492.

105. Tang, W., Shin, J.D., Frank, L.M., and Jadhav, S.P. (2017). Hippocampal-Prefrontal Reactivation during Learning Is Stronger in Awake Compared with Sleep States. J. Neurosci. *37*, 11789–11805. https://doi.org/10.1523/JNEUROSCI.2291-17.2017.

106. Morris, J.K., Vidoni, E.D., Johnson, D.K., Van Sciver, A., Mahnken, J.D., Honea, R.A., Wilkins, H.M., Brooks, W.M., Billinger, S.A., Swerdlow, R.H., and Burns, J.M. (2017). Aerobic exercise for Alzheimer's disease: A randomized controlled pilot trial. PLoS One *12*, e0170547. https://doi.org/10.1371/journal.pone.0170547.

107. Scarmeas, N., Stern, Y., Tang, M.X., Mayeux, R., and Luchsinger, J.A. (2006). Mediterranean diet and risk for Alzheimer's disease. Ann. Neurol. *59*, 912–921. https://doi.org/10.1002/ana.20854.

108. Mangialasche, F., Solomon, A., Winblad, B., Mecocci, P., and Kivipelto, M. (2010). Alzheimer's disease: clinical trials and drug development. Lancet Neurol. *9*, 702–716. https://doi.org/10.1016/S1474-4422(10)70119-8.

109. Tuszynski, M.H., Thal, L., Pay, M., Salmon, D.P., U, H.S., Bakay, R., Patel, P., Blesch, A., Vahlsing, H.L., Ho, G., et al. (2005). A phase 1 clinical trial of nerve growth factor gene therapy for Alzheimer disease. Nat. Med. *11*, 551–555. https://doi.org/10.1038/nm1239.

110. Pople, C.B., Meng, Y., Li, D.Z., Bigioni, L., Davidson, B., Vecchio, L.M., Hamani, C., Rabin, J.S., and Lipsman, N. (2020). Neuromodulation in the Treatment of Alzheimer's Disease: Current and Emerging Approaches. J. Alzheimers Dis. *78*, 1299–1313. https://doi.org/10.3233/JAD-200913.

111. Vogt, N.M., Kerby, R.L., Dill-McFarland, K.A., Harding, S.J., Merluzzi, A.P., Johnson, S.C., Carlsson, C.M., Asthana, S., Zetterberg, H., Blennow, K., et al. (2017). Gut microbiome alterations in Alzheimer's disease. Sci. Rep. *7*, 13537. https://doi.org/10.1038/s41598-017-13601-y.

112. Cacucci, F., Yi, M., Wills, T.J., Chapman, P., and O'Keefe, J. (2008). Place cell firing correlates with memory deficits and amyloid plaque burden in Tg2576 Alzheimer mouse model. Proc. Natl. Acad. Sci. USA *105*, 7863–7868. https://doi.org/10.1073/pnas.0802908105.

113. Zhang, H., Chen, L., Johnston, K.G., Crapser, J., Green, K.N., Ha, N.M.L., Tenner, A.J., Holmes, T.C., Nitz, D.A., and Xu, X. (2023). Degenerate mapping of environmental location presages deficits in object-location encoding and memory in the 5xFAD mouse model for Alzheimer's disease. Neurobiol. Dis. *176*, 105939. https://doi.org/10.1016/j.nbd.2022.105939.

114. Jun, H., Bramian, A., Soma, S., Saito, T., Saido, T.C., and Igarashi, K.M. (2020). Disrupted Place Cell Remapping and Impaired Grid Cells in a Knockin Model of Alzheimer's Disease. Neuron *107*, 1095–1112.e6. https://doi.org/10.1016/j.neuron.2020.06.023.

115. Ying, J., Keinath, A.T., Lavoie, R., Vigneault, E., El Mestikawy, S., and Brandon, M.P. (2022). Disruption of the grid cell network in a mouse model of early Alzheimer's disease. Nat. Commun. *13*, 886. https://doi.org/10.1038/s41467-022-28551-x.

116. Mably, A.J., Gereke, B.J., Jones, D.T., and Colgin, L.L. (2017). Impairments in spatial representations and rhythmic coordination of place cells in the 3xTg mouse model of Alzheimer's disease. Hippocampus *27*, 378–392. https://doi.org/10.1002/hipo.22697.

117. Cayzac, S., Mons, N., Ginguay, A., Allinquant, B., Jeantet, Y., and Cho, Y.H. (2015). Altered hippocampal information coding and network synchrony in APP-PS1 mice. Neurobiol. Aging *36*, 3200–3213. https://doi.org/10.1016/j.neurobiolaging.2015.08.023.

118. Kim, J.J., and Fanselow, M.S. (1992). Modality-specific retrograde amnesia of fear. Science *256*, 675–677. https://doi.org/10.1126/science.1585183.

119. Phillips, R.G., and LeDoux, J.E. (1992). Differential contribution of amygdala and hippocampus to cued and contextual fear conditioning. Behav. Neurosci. *106*, 274–285. https://doi.org/10.1037//0735-7044.106.2.274.

120. Kimura, R., and Ohno, M. (2009). Impairments in remote memory stabilization precede hippocampal synaptic and cognitive failures in 5XFAD Alzheimer mouse model. Neurobiol. Dis. *33*, 229–235. https://doi.org/10.1016/j.nbd.2008.10.006.

121. Corcoran, K.A., Lu, Y., Turner, R.S., and Maren, S. (2002). Overexpression of hAPPswe impairs rewarded alternation and contextual fear conditioning in a transgenic mouse model of Alzheimer's disease. Learn. Mem. *9*, 243–252. https://doi.org/10.1101/lm.51002.

122. Thorndike, E. (1899). Instinct. In Biological Lectures from the Marine Laboratory at Woods Holl (Ginn & Company), pp. 57–67.

123. Espana, J., Gimenez-Llort, L., Valero, J., Minano, A., Rabano, A., Rodriguez-Alvarez, J., LaFerla, F.M., and Saura, C.A. (2010). Intraneuronal beta-amyloid accumulation in the amygdala enhances fear and anxiety in Alzheimer's disease transgenic mice. Biol. Psychiatry *67*, 513–521. https://doi.org/10.1016/j.biopsych.2009.06.015.

124. He, Z., Guo, J.L., McBride, J.D., Narasimhan, S., Kim, H., Changolkar, L., Zhang, B., Gathagan, R.J., Yue, C., Dengler, C., et al. (2018). Amyloid-beta plaques enhance Alzheimer's brain tau-seeded pathologies by facilitating neuritic plaque tau aggregation. Nat. Med. *24*, 29–38. https://doi.org/10.1038/nm.4443.

125. Kromer Vogt, L.J., Hyman, B.T., Van Hoesen, G.W., and Damasio, A.R. (1990). Pathological alterations in the amygdala in Alzheimer's disease. Neuroscience *37*, 377–385. https://doi.org/10.1016/0306-4522(90)90408-v.

126. Trejo-Lopez, J.A., Yachnis, A.T., and Prokop, S. (2022). Neuropathology of Alzheimer's Disease. Neurotherapeutics *19*, 173–185. https://doi.org/10.1007/s13311-021-01146-y.

127. Burgos-Robles, A., Kimchi, E.Y., Izadmehr, E.M., Porzenheim, M.J., Ramos-Guasp, W.A., Nieh, E.H., Felix-Ortiz, A.C., Namburi, P., Leppla, C.A., Presbrey, K.N., et al. (2017). Amygdala inputs to prefrontal cortex guide behavior amid conflicting cues of reward and punishment. Nat. Neurosci. *20*, 824–835. https://doi.org/10.1038/nn.4553.

128. Pedigo, S.F., Song, E.Y., Jung, M.W., and Kim, J.J. (2006). A computer vision-based automated Figure-8 maze for working memory test in rodents. J. Neurosci. Methods *156*, 10–16. https://doi.org/10.1016/j.jneumeth.2006.01.029.

129. Kim, E.J., Kim, E.S., Covey, E., and Kim, J.J. (2010). Social transmission of fear in rats: the role of 22-kHz ultrasonic distress vocalization. PLoS One *5*, e15077. https://doi.org/10.1371/journal.pone.0015077.

130. Blanchard, R.J., and Blanchard, D.C. (1969). Crouching as an index of fear. J. Comp. Physiol. Psychol. *67*, 370–375. https://doi.org/10.1037/h0026779.

STAR★METHODS

KEY RESOURCES TABLE

REAGENT or RESOURCE	SOURCE	IDENTIFIER
Antibodies		
Mouse Anti-Human Aβ Monoclonal Antibody	Medimabs	RRID: AB_1807985
Goat Anti-Mouse IgG H&L (Alexa Fluor® 568)	Abcam	RRID: AB_2895153
Experimental models: Organisms/strains		
B6SJL-Tg(APPSwFlLon, PSEN1*M146L*L286V)6799Vas/Mmjax	The Jackson Laboratory	RRID: MMRRC_034840-JAX
B6.Cg-Tg(APPSwFlLon, PSEN1*M146L*L286V) 6799Vas/Mmjax	The Jackson Laboratory	RRID: MMRRC_034848-JAX
Software and algorithms		
MATLAB	The MathWorks	http://www.mathworks.com/products/matlab/; RRID: SCR_001622
Custom MATLAB code for single-unit and LFP data analyses	This paper	https://github.com/KimLab-UW-NSB/5xfad-hpc-pfc-neural-dynamics.git
GraphPad Prism	GraphPad software	http://www.graphpad.com/; RRID: SCR_002798
R	R Foundation	http://www.r-project.org/; RRID: SCR_001905
ImageJ	National Institutes of Health	https://imagej.net/ij/; RRID: SCR_003070
Cheetah	NeuraLynx, Inc.	https://neuralynx.fh-co.com/research-software/cheetah/
Spikesort3D	NeuraLynx, Inc.	https://neuralynx.fh-co.com/research-software/spikesort-3d/; RRID: SCR_014478
NeuroExplorer	Nex Technologies	https://www.neuroexplorer.com/; RRID: SCR_001818
bioRender	bioRender	https://www.biorender.com/

EXPERIMENTAL MODEL AND STUDY PARTICIPANT DETAILS

Animals

5XFAD transgenic mice, which overexpress amyloid precursor protein (APP) and presenilin 1 (PS1), along with their WT littermate mice counterparts (aged 4–8 weeks, both sexes), were used in this study. Mouse strains B6SJL-Tg(APPSwFlLon, PSEN1*M146L*L286V)6799Vas/Mmjax (RRID: MMRRC_034840-JAX) and B6.Cg-Tg(APPSwFlLon, PSEN1*M146L*L286V)6799Vas/Mmjax (RRID: MMRRC_034848-JAX) were obtained from the NIH-funded MMRRC at The Jackson Laboratory, originally donated by Dr. Robert Vassar, Northwestern University.[47] Initially, these animals were group-housed in a climate-controlled vivarium under a reversed 12-h light/dark cycle (lights on at 7 PM), accredited by the Association for Assessment and Accreditation of Laboratory Animal Care (AAALAC). Upon initiation of experimental procedures, 4-9-month-old mice were individually housed and placed on a standard food-deprivation schedule, with *ad libitum* access to water, to maintain ~85% of their normal body weight. A total of 17 5XFAD and 17 WT mice were assigned to the escalating predatory risk task (Figure 1), while a separate cohort (5XFAD, $n = 11$; WT, $n = 6$) underwent combined tetrode recording and conditional predatory risk testing (Figure 2), as detailed below. All experiments were conducted during the dark phase in strict accordance with the guidelines of the University of Washington Institutional Animal Care and Use Committee (IACUC protocol #: 4040-01).

METHOD DETAILS

Surgery

Under isoflurane anesthesia, animals were secured in a stereotaxic instrument (Kopf) for the implantation of a microdrive array containing individually movable tetrodes. The tetrodes targeted the right dHPC (AP: −1.8, ML: +1.7, DV: −1.3; four tetrodes) and mPFC (AP: +1.8, ML: +0.3, DV: −1.2; four tetrodes). The tetrodes were fabricated from formvar-insulated nichrome wire (14 μm diameter; Kanthal) and gold-plated to a final impedance of 100–300 kΩ (measured at 1 kHz). The microdrive assembly was secured with dental cement and bone screws. A recovery period of at least one week preceded the initiation of behavioral experiments and recording sessions.

Escalating predatory risk

This task was conducted in a custom-built apparatus consisting of a nest area (inner dimensions: 14 cm L × 45 cm W × 61 cm H; luminance: 2.2 lux) and an adjacent foraging space (104 cm L × 45 cm W × 61 cm H; luminance: 5.0 lux; background noise: 72-dB white noise). The environment was monitored using the ANY-maze system (Stoelting Co.) and a ceiling-mounted HD webcam (C910; Logitech) for video tracking at 30 fps (Figure 1A). The task consisted of three phases: habituation, baseline foraging, and weasel predator testing.

During habituation, hunger-motivated mice were acclimated by being placed in the nest with 20 food pellets (45 mg each, F0165, Bio-Serv) for 30 min/day over two days. For baseline foraging, mice were provided with two 45-mg pellets in the nest. After consuming these, they were given access to the foraging area via an open gateway to retrieve pellets placed at distances of 12.7 cm (S), 25.4 cm (M), and 38.1 cm (L) from the nest. Each daily session included three trials for four consecutive days.

The predator testing phase began with mice foraging for a pellet placed 38.1 cm from the nest in three consecutive trials. Subsequent trials introduced a taxidermy weasel mounted on a wheeled frame positioned at the opposite end of the foraging space. As the mouse approached the pellet within ~12.7 cm, the weasel was activated to surge forward 30.4 cm toward the pellet at 60 cm/s using a pneumatic actuator, then automatically returned to its starting position. Each trial ended either when the mouse successfully secured the pellet or after 3 min had elapsed. This process was repeated for pellet placements at 25.2 cm and 12.7 cm.

Conditional predatory risk

Adapted from a figure-eight maze,[128] this T-maze setup features a nest area at the base (dimensions: 92 cm L × 92 cm W × 79 cm H; luminance: 7 lux) and two lateral goal arms, each equipped with a concealed puppet eagle predator near a designated pellet zone (Figure 2A). Movement was tracked using headstage-mounted LEDs and integrated with the ANY-maze (Stoelting Co.) and Cheetah (NeuraLynx, Inc.) systems. This maze design ensured consistent location visits, enabling optimal place cell analysis.

The task protocol comprised four phases: habituation, shaping, baseline foraging, and predator testing, with tetrodes adjusted toward the target areas as detailed in the 'Unit recording and analyses' section. During habituation (two days), animals were placed in the nest for 30 min/day with ten grain (45 mg, F0165, Bio-Serv) and ten chocolate (45 mg, F0299, Bio-Serv) pellets to facilitate acclimation. The shaping phase lasted three days. Mice received one grain and one chocolate pellet in the nest. After consumption, the nest gate opened, guiding them to retrieve a pellet at increasing distances. Each arm was consistently assigned a specific pellet type. After a forced-arm retrieval and pellet consumption, the next trial began on the opposite arm. During baseline foraging, two pellets were provided in the nest. After consumption, the nest gate opened, allowing mice to choose between the left and right arm pellets. Choosing one pellet triggered the closure of the opposite arm gate. Each daily session included 6 trials, lasting for an average of 8.6 ± 1.03 days. Predator testing sessions, during which neural recordings were conducted, included pre-predator (8–14 trials), predator (3–10 trials), and post-predator (10 min nest period) phases. During predator trials, when mice approached the preferred pellet, a puppet eagle surged forward (15.2 cm at 38 cm/s via a linear actuator). In contrast, when mice approached the non-preferred pellet, the predator remained hidden behind a black plastic block. Pellet preference was quantified using a Preference Index (PI), defined as the ratio of preferred pellet choices to total pellet choices.

Contextual fear conditioning

After completing the conditional predatory risk task, 5XFAD and WT mice were placed in a standard operant chamber with a stainless-steel grid floor (5 mm diameter rods spaced 1 cm apart).[100] Following a 3-min baseline period, three unsignaled footshocks (0.7 mA, 1 s) were administered at 1-min intervals. Postshock freezing was assessed between each shock. The next day, mice were returned to the same chamber, and their conditioned freezing response to the context was measured for 3 min before administering another set of 3 unsignaled shocks and assessing postshock freezing. An uninformed observer used a custom-written computer-assisted scoring program (written in C language) to manually record the duration of freezing behavior via keystrokes on a computer keyboard.[129] Freezing was defined as the absence of any visible movement in the body and vibrissae, except for respiratory movements.[130] The program applied a continuous inactivity threshold of 2 s or more to identify freezing. The percentage of freezing was calculated by dividing the total duration of freezing by the total observation time and multiplying by 100.

Electrophysiological recording and analysis

Data acquisition

Single-unit and local field potential (LFP) signals were amplified (10,000×), filtered (unit: 600 Hz–6000 Hz; LFPs: 0.1 Hz–1000 Hz), and digitized at 32 kHz using the Cheetah data acquisition system (NeuraLynx). Unit isolation was performed using an automatic spike-sorting program (SpikeSort 3D; NeuraLynx) followed by manual cluster cutting, following protocols described in previous studies.[43,44] Raster plots and peristimulus time histograms were generated using NeuroExplorer (Nex Technologies).

Place cell analysis

Place cells were identified based on criteria established in prior research.[44,66] Units were classified as place cells if they exhibited stable, well-discriminated complex spike waveforms, a refractory period of at least 1 ms, peak firing rates >2 Hz in any session, and spatial information >0.5 bits/s in any session. Place cells were categorized according to the peak positions of their place fields during the pre-predator session as follows: nest cells (maximal firing in the nest), center cells (maximal firing in the center zone), risky arm cells (maximal firing in the maze arm near the threat), and safe arm cells (maximal firing in the maze arm away from the

threat). A pixel-by-pixel spatial correlation analysis was performed using a customized R program to calculate the similarity of place maps between the pre-predator and predator sessions for each place cell. The correlation value (r) was transformed into a Fisher Z′ score for parametric comparisons between cell types. Additionally, the program calculated the distance between each cell's peak firing locations across sessions. The maximal firing locations (x, y coordinates) were identified for each session, and the distance (in cm) between these points was calculated to measure positional shifts of place fields from the pre-predator to predator sessions.

Cross-correlogram (CC) analysis

CC of simultaneously recorded dHPC and mPFC units were generated using NeuroExplorer, following established methods.[43,66] CCs were constructed with dHPC cells as the reference, using a 10-ms bin width for two time epochs: *pre-turn epoch*$_{pre}$ (a 3-s epoch before the animal turned at the end of the center zone toward one of the arms during the pre-predator session) and *pre-turn epoch*$_{predator}$ (a 3-s epoch before the turn during the predator session). To avoid false correlations due to covariation or nonstationary firing rates between the dHPC and mPFC, a 'Shift-Predictor' correction was applied, with trial shuffles performed 100 times.[43] Each shift-predictor correlogram was subtracted from its respective raw correlogram, and Z-scores were calculated using the mean and standard deviation of the corrected CCs. A neural pair was deemed significantly correlated if the peak *Z* score exceeded 3. Additional criteria required that dHPC and mPFC firing rates during pre-turn periods for both the pre-predator and predator sessions be above 0.2 Hz, and the peak of the CC had to fall within a ±100 ms testing window relative to the reference spikes.

LFP and SWR analysis

LFP signals from a single channel of each animal's dHPC electrodes were band-pass filtered between 150 and 250 Hz using a zero-phase digital filter to minimize phase distortions. The envelope of these high-frequency oscillations was extracted using the Hilbert transform, providing a precise measure of their amplitude. The resulting envelope was smoothed with a Gaussian-weighted moving average over a 40 ms window. SWR events were detected when the smoothed envelope exceeded a threshold of 4 standard deviations above the mean amplitude. The event ended when the amplitude fell below 2 standard deviations, ensuring precise delineation of event boundaries. Only SWR events with durations over 15 ms were included in the analysis. During the post-predator session in the nest, movement states for SWR analysis were classified as moving (velocity $\geq$5 cm/s) or not moving (velocity <5 cm/s).[71]

SWR modulation of unit activity analysis

To assess the modulatory effects of SWRs on dHPC and mPFC unit activity, unit firing rates were normalized to pre-SWR baseline periods (dHPC: −500 to −250 ms; mPFC: −1000 to −500 ms). A neuron was classified as significantly activated if its peak Z-score exceeded 3 within a specified time window around SWR onset (dHPC: ±100 ms or ±250 ms; mPFC: ±250-ms or ±500 ms). All analyses were conducted using MATLAB 2024 Signal Processing Toolbox, which provided the necessary tools for detailed signal examination and processing.

Phase-locking analysis

Hippocampal LFPs were band-pass filtered between 4-12 Hz using a zero-phase-delay Butterworth filter (4th order) implemented with the *filtfilt* function in MATLAB (MathWorks) to prevent phase distortion. The instantaneous phase of the theta rhythm was extracted using the Hilbert transform. For each prefrontal cortical neuron, spike times were assigned corresponding theta phase via linear interpolation between the LFP time series and spike timestamps. Phase-locking significance was assessed using the Rayleigh test for circular uniformity (via the *circ_rtest* function, Circular Statistics Toolbox), which evaluates whether spike phases are uniformly distributed around the theta cycle. Neurons with $p < 0.05$ (Rayleigh test) and at least 40 spikes[81–83] were considered significantly phase-locked to the hippocampal theta rhythm. The strength of phase-locking was quantified by the Mean Resultant Length (MRL), calculated with the *circ_r* function. MRL values range from 0 (uniform distribution, no phase-locking) to 1 (perfect phase-locking). The preferred phase of firing was determined using the circular mean phase via the *circ_mean* function.

Histology

After concluding the experiment, electrolytic lesions were created by applying a 10 μA current for 10 s to the tetrode tips to mark electrode placements. Mice were then euthanized with an overdose of Beuthanasia and perfused intracardially with phosphate-buffered saline (PBS), followed by fixation with 4% paraformaldehyde in PBS. Extracted brains were stored overnight at 4°C in fixative, then transferred to 10%, 20%, and 30% sucrose solutions until they sank. For Aβ immunostaining, transverse brain sections (30 μm) were rinsed in PBS and incubated for 1 h in 5% normal goat serum with 0.5% Triton X- in PBS to block non-specific binding. The sections were then incubated overnight at 4°C with Aβ-specific mouse monoclonal antibody (1:1000, MediMabs, McSA1). After thorough washing, sections were incubated with a goat anti-mouse secondary antibody conjugated to Alexa Fluor 568 (1:250, Abcam, ab175473) for 2 h at room temperature. The prepared sections were mounted on slides and cover slipped with Flouromount-G™ containing DAPI (eBioscience) for nuclear staining. Imaging was performed using a Keyence BZ-X800E microscope. Image analysis was conducted using ImageJ software (NIH, version 1.54d). A separate set of brain sections was mounted onto gelatinized slides and stained with Cresyl violet and Prussian blue to confirm the precise locations of the tetrode tips.

QUANTIFICATION AND STATISTICAL ANALYSIS

Statistical analyses analysis

Statistical significance was assessed using a range of tests tailored to the diverse data structures in the study. These tests included one-way ANOVAs for group comparisons, mixed-design ANOVAs for analyses incorporating both within- and between-subject variables, Pearson's correlation, unpaired t-tests, and paired t-tests. Post hoc analyses, when required, were conducted using Tukey's test or Fisher's least significant difference test. The Greenhouse-Geisser correction was applied to account for sphericity violations. Comprehensive details for each statistical analysis are provided in Table S1. Statistical significance was defined as $p < 0.05$. Statistical analyses and graph generation were performed using SPSS (ver. 19), custom MATLAB codes, GraphPad Prism (ver. 9.00), and NeuroExplorer (ver. 5.030).